Journal of Medicinal Chemistry

Drug Annotation

Cite This: J. Med. Chem. XXXX, XXX, XXX−XXX

pubs.acs.org/jmc

Discovery of Risdiplam, a Selective Survival of Motor Neuron-2 (*SMN2*) Gene Splicing Modifier for the Treatment of Spinal Muscular Atrophy (SMA)

Hasane Ratni,*[,†] Martin Ebeling,[†] John Baird,[‡] Stefanie Bendels,[†] Johan Bylund,[†] Karen S. Chen,[§] Nora Denk,[†] Zhihua Feng,[∥] Luke Green,[†] Melanie Guerard,[†] Philippe Jablonski,[†] Bjoern Jacobsen,[†] Omar Khwaja,[†] Heidemarie Kletzl,[†] Chien-Ping Ko,[∥] Stefan Kustermann,[†] Anne Marquet,[†] Friedrich Metzger,[†] Barbara Mueller,[†] Nikolai A. Naryshkin,[‡] Sergey V. Paushkin,[§] Emmanuel Pinard,[†] Agnès Poirier,[†] Michael Reutlinger,[†] Marla Weetall,[‡] Andreas Zeller,[†] Xin Zhao,[‡] and Lutz Mueller*[,†]

[†]F. Hoffmann-La Roche Ltd., pRED, Pharma Research & Early Development, Roche Innovation Center Basel, Grenzacherstrasse 124, 4070 Basel, Switzerland

[‡]PTC Therapeutics, Inc., 100 Corporate Court, South Plainfield, New Jersey 07080, United States

[§]SMA Foundation, 888 Seventh Avenue, Suite 400, New York, New York 10019, United States

[∥]Section of Neurobiology, Department of Biological Sciences, University of Southern California, Los Angeles, California 90089, United States

Supporting Information

ABSTRACT: SMA is an inherited disease that leads to loss of motor function and ambulation and a reduced life expectancy. We have been working to develop orally administrated, systemically distributed small molecules to increase levels of functional SMN protein. Compound **2** was the first SMN2 splicing modifier tested in clinical trials in healthy volunteers and SMA patients. It was safe and well tolerated and increased SMN protein levels up to 2-fold in patients. Nevertheless, its development was stopped as a precautionary measure because retinal toxicity was observed in cynomolgus monkeys after chronic daily oral dosing (39 weeks) at exposures in excess of those investigated in patients. Herein, we describe the discovery of **1** (risdiplam, RG7916, RO7034067) that focused on thorough pharmacology, DMPK and safety characterization and optimization. This compound is undergoing pivotal clinical trials and is a promising medicine for the treatment of patients in all ages and stages with SMA.

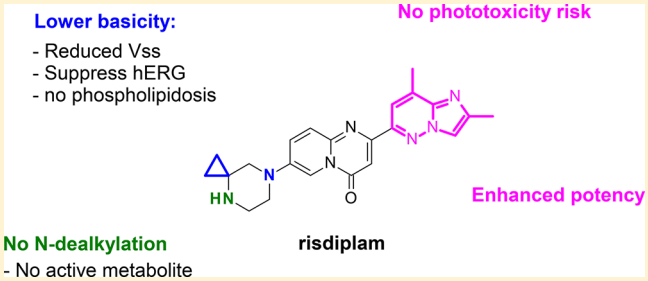

INTRODUCTION

Spinal muscular atrophy (SMA)[1] is an autosomal recessive neuromuscular disorder characterized by the progressive loss of spinal motor neurons leading to muscle weakness. It is the leading genetic cause of mortality in infants and young children, with an incidence of 1 in 11 000 live births.[2] SMA manifests in various degrees of severity ranging from type 1 (patients never achieve independent sitting) to type 2 (patients can sit but not stand or walk) and type 3 (patients achieve walking ability), all of which have in common clinical signs including hypotonia, muscle weakness and atrophy, and impaired mobility.

SMA is caused by a homozygous deletion or mutation of the survival of motor neuron 1 (*SMN1*) gene on chromosome 5q (locus 5q13) which encodes survival motor neuron protein (SMN), an essential protein for normal development and functional homeostasis in all species,[3] expressed in both neuronal and non-neuronal cells. Most humans carry a second, very closely related gene *SMN2* that also can produce SMN protein; however, its level is mainly driven by the *SMN1* gene. The *SMN2* gene, due to a translationally synonymous C- to T-mutation in exon 7, encodes a pre-mRNA that undergoes alternative splicing that excludes exon 7 from the majority of the mRNA. This *SMN2*Δ*7* mRNA produces a rapidly degrading SMNΔ7 protein, whereas the reduced quantities of full length SMN2 mRNA generate insufficient levels of wild type full length SMN protein. All SMA patients (with no functional *SMN1* gene) have at least one *SMN2* copy, and some have up to six copies in a somatic cell.[4] Our strategy to treat SMA has focused on the discovery and development of orally bioavailable and brain penetrant small molecules that shift the outcome of *SMN2* alternative splicing toward the production of full length *SMN2* mRNA increasing functional SMN protein levels. The hallmark of SMA is the progressive degeneration of α-motor neurons in the brain stem and spinal cord that causes muscle atrophy and disease-related complications that can impact survival. However,

Received: May 8, 2018

DOI: 10.1021/acs.jmedchem.8b00741
J. Med. Chem. XXXX, XXX, XXX−XXX

more and more data suggest that SMA is not only a disease of motor neurons. SMA is increasingly described as a disease affecting tissues and cell types beyond the motor neuron. This then strongly suggest that an effective treatment may require body-wide correction of SMN protein levels to achieve a complete reversal or amelioration of the disease state. Hence we are looking for small molecule increasing SMN protein in both the CNS and peripheral organs and tissues upon oral administration.

In recent years, a number of therapeutic options for SMA have been assessed,[5] and among them the modification of *SMN2* alternative splicing appears highly promising. It can be achieved either by antisense oligonucleotides (ASOs)[6] (nusinersen approved by U.S. FDA in December 2016) that currently require intrathecal administration or advantageously by small molecules upon oral delivery leading to SMN protein level increases in both the CNS and peripheral organs and tissues as initially reported by us[7] and recently by others (5-(1*H*-pyrazol-4-yl)-2-[6-[(2,2,6,6-tetramethyl-4-piperidyl)oxy]pyridazin-3-yl]phenol (branaplam, LMI070), currently in phase 2 clinical trials).[8]

In this paper, we describe the path from compound **2** (RG7800, RO6885247),[9] the first molecule which entered human clinical trials in SMA, to the discovery of compound **1** (risdiplam, RG7916, RO7034067, 7-(4,7-diazaspiro[2.5]octan-7-yl)-2-(2,8-dimethylimidazo[1,2-*b*]pyridazin-6-yl)pyrido[1,2-*a*]pyrimidin-4-one) currently undergoing pivotal clinical studies in SMA patients (Figure 1). We utilized state-of-the-art optimization and characterization of the pharmacology, DMPK, and nonclinical safety.

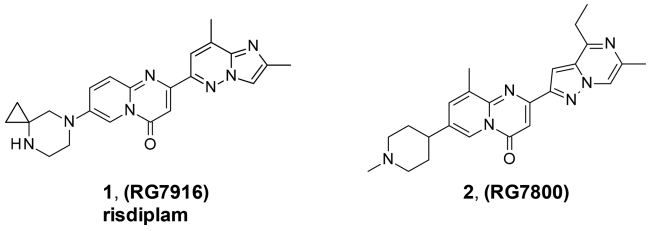

Figure 1. Structures of compounds **1** and **2**.

BACKGROUND

Characterization of Compound 2. A first-in-human study to assess compound **2** for safety, tolerability, pharmacokinetics (PK), and pharmacodynamics (PD) in healthy subjects was performed. Single oral doses were administered to healthy male subjects in a single-ascending-dose, placebo controlled, double blind study. *SMN1* full length, *SMN2* full length, and *SMN*Δ7 (generated predominantly by the *SMN2* gene) mRNA levels were quantified in whole blood samples using a newly developed multiplex RT-qPCR assay. Compound **2** was safe and well tolerated in this study at all doses tested, with the highest dose selected being determined by animal no adverse effect data and the ability to generate reliable pharmacodynamic effects (RNA splicing data in blood cells as biomarker). The plasma exposure increased in a slightly more than dose proportional manner. The peak plasma concentration of compound **2** was reached at 5−8 h after dose with a terminal half-life of 120 h. Due to long half-life, subjects showed exposure to compound **2** in plasma for more than 2 weeks. A dose- and exposure-dependent effect on *SMN2* exon 7 splicing in whole blood was observed: the levels of full length *SMN2* mRNA increased, and the levels of *SMN2*Δ*7* mRNA decreased, with no detectable change in *SMN1* full length mRNA levels. Those results supported the evaluation of compound **2** in SMA patients to assess its safety and confirmed proof of mechanism measuring its effect on SMN2 exon 7 splicing and on SMN protein levels in whole blood.[10] An increase in full length *SMN2* mRNA levels and up to a 2-fold increase in SMN protein levels relative to those at baseline after 12 weeks of treatment were achieved. However, this clinical study was put on hold as a precautionary measure due to safety findings in cynomolgus monkeys (nonreversible histological findings in the retina) in the long term chronic toxicity study (39 weeks) performed in parallel to the clinical trial. Exposure levels of compound **2** in this long-term chronic preclinical toxicity study were however considerably higher than those reached in the clinical study. However, it seemed not feasible to explore the full therapeutic potential of compound **2** while still maintaining a safety margin to the animal toxicity findings.

Selectivity of 2. This proof of mechanism achieved in SMA patients supported the subsequent identification of a molecule with improved properties. Efforts focused on increasing further the therapeutic index and improving the PK profile.

One parameter evaluated was selectivity. We recently reported on a transcriptional profiling analysis performed in PNN1-46 SMA patient-derived fibroblasts treated with various compounds that all had an effect on SMN2 splicing.[11] Going through the list of genes whose splicing was affected by at least one such compound (Figure 3b of our previously published work;[11] also see Figure 14), we identified several genes of particular relevance for their established functional roles in cell cycle regulation or cell death signaling. The functions of these genes, such as *FOXM1* and *MADD*, were consistent with phenotypes seen in in vitro and animal toxicity studies in the form of (stage-specific) cell cycle arrest, micronucleus induction, and apoptosis formation as described later in this paper. FOXM1, forkhead box protein M1, encodes a key cell cycle regulator. FOXM1 protein is critically required for cell division and is highly expressed in rapidly dividing cells, such as those found in the gastrointestinal tract, male germ cells, skin, and blood cell progenitors in the bone marrow. Knock-down of *FOXM1* or a change in its splice variants can lead to mitotic arrest and apoptosis, depending on the stage of the cell cycle. The transcriptionally inactive FOXM1a variant contains exon A2 (full length), and the transcriptionally active FOXM1b/c variants lack exon A2 (ΔA2). There is also a third, recently described *FOXM1ΔC* isoform.[12] *FOXM1ΔC* is expressed in several cancer cell lines, interferes with normal cell cycle progression, induces chromosomal instability and aneuploidy. Using RT-qPCR with specific primers for FOXM1a (full length) and FOXM1b/c (ΔA2), the change in the alternative splicing pattern of FOXM1 after treatment with compound **2** in SMA patient-derived fibroblasts was confirmed with a *FOXM1a* EC_{50} of 247 nM (±60 nM) and *FOXM1b/c* EC_{50} 352 nM (±49 nM), respectively. For comparison, the *SMN2* splicing activity (FL mRNA in HEK293H) of compound **2** was 23 nM. We also evaluated the effect of compound **2** on the expression level of *FOXM1* mRNA variants (*FOXM1b/c*) in human and cynomolgus monkey induced pluripotent stem cells (iPSCs). A similar potency was observed with an IC_{50} of 1.85 μM and 0.90 μM in human and cynomolgus monkey iPSCs, respectively. These data confirm similarities in responses of human and cynomolgus monkey cells toward changes in splice variants of *FOXM1*, which is particularly important as cynomolgus

DOI: 10.1021/acs.jmedchem.8b00741
J. Med. Chem. XXXX, XXX, XXX−XXX

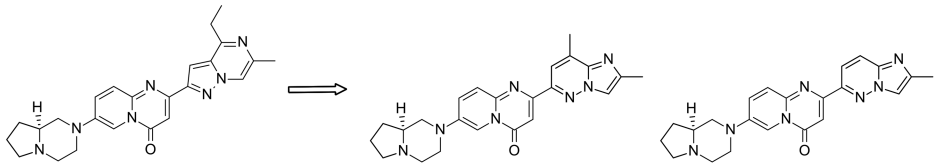

3 4 5

Compd	3	4	5
SMN2 splicing $EC_{1.5x}$ [nM]	40	2	3
SMN protein $EC_{1.5x}$ [nM]	163	22	20

Figure 2. Structures of compounds **3**, **4**, and **5** with a more potent imidazopyridazine moiety.

monkeys were used for toxicity characterization of compound **1** and sufficient margins in terms of safety were established in vivo to study the full therapeutic potential of compound **1** in patients.

Nonclinical Pharmaceutical Evaluation and Safety of 2. Other pharmaceutical and safety-related properties were also evaluated. The effect of compound **2** on the hERG channel was assessed at 37 °C giving an IC_{50} and IC_{20} of 1.8 μM and 0.5 μM, respectively. A telemetry study was performed in cynomolgus monkeys in which a mild QTC interval prolongation of at most 10 ms was observed only at the highest dose tested. The exposure at the highest dose in cynomolgus monkeys reached the IC_{20}, and hence in vivo results were in line with the IC_{20} of the hERG channel interaction in vitro and thus expected. Clinical investigations and management of such effects in the clinic were put in place.

In an in vitro phototoxicity assessment of compound **2** using the standard neutral red uptake assay upon UVA irradiation in 3T3 fibroblasts an IC_{50} of 330 nM was measured (IC_{50} > 10 μM in the dark). The phototoxic potential was subsequently confirmed in rats in vivo. Clinical safety measures were put in place for the trials with compound **2**.

As part of the testing for genotoxic activity, compound **2** was found to be negative in the bacterial reverse mutation assay. However, increased frequencies of micronucleated cells were observed both in vitro in mammalian cells (mouse and human cells) and in vivo in rats upon oral dosing. The increased frequency of micronucleated cells can be expected based on the changes in *FOXM1* splicing observed in the presence of compound **2**. We also observed changes in male germ cell in vivo in rats and cynomolgus monkeys after at least seven once-daily oral doses of compound **2**. Similar observations with compound **1** were made, for which the mechanism is further discuss herein after.

Microscopic examination in cynomolgus monkey tissue revealed stage- and cell-specific germ cell degeneration in the testes in males. Staging analysis of the germ cell degeneration was performed, and it turned out that the arrest occurred primarily in the pachytene stage of meiosis I and associated with decreased sperm count, increased abnormal sperms, and reduced testes size. In line with this observation, testis findings fully reversed or showed ongoing recovery (normalization of sperm count, sperm morphology and testis size, absence of germ cell degeneration) following an extended period of observation after treatment cessation. The master cell cycle regulating factor FOXM1 (also termed HFH11) is known to be highly expressed in spermatocytes but not spermatogonia of the testis.[13] Thus, the effect of treatment of cynomolgus monkeys with compound **2** on testes is stage-specific and reversible. Similar findings were observed for compound **1**.

Consistent with the large volume of distribution of compound **2** (V_{ss} = 29 L/kg in rat) and its basic charge, histopathological observations of epithelial vacuolation and foamy macrophages were observed suggestive of phospholipidosis in several tissues in the rat. The effect was less pronounced than with other compounds in the same chemistry series. Overall, a large volume of distribution appeared to be the key driver of phospolipidosis. Thus, reduction of V_{ss} was part of the further optimization process to arrive at compound **1**.

Possible improvement of the PK profile of compound **2** initially consisted of shortening the half-life as well as reducing its volume of distribution (V_{ss}). We have reported a terminal half-life of around 120 h in healthy adult humans. This is consistent with our observation in rats and cynomolgus monkeys with a respective half-life of 19 h and 42h after oral dosing and a V_{ss} of around 20 to 30 L/kg for both species.

COMPOUND DESIGN AND OPTIMIZATION RESULTING IN DISCOVERY OF 1

As a continuation of our efforts to discover a *SMN2* splicing modifier drug candidate with an improved safety, pharmacokinetic and pharmacodynamic profile suitable for the chronic treatment of SMA patients, we evaluated a novel class of benzamide derivatives which has been recently reported.[14] While this class initially held some promises, such as absence of phototoxicity, different chemotype and first prototypes displaying good in vivo efficacy, this series was ultimately terminated. The in vivo efficacy could not be further improved, with the best derivatives being less potent than compound **2** and offering no advantage in terms of selectivity. We therefore kept our focus on the pyridopyrimidinone series, from which our first clinical candidate was identified.

To increase the therapeutic window versus nontarget related potential side effect (e.g., hERG channel interaction, phospholipidosis, phototoxicity), we focused on changing key elements in the molecules to reduce basicity (bpKa: basic pK_a), volume of distribution, and UV absorption and at the same to improve the potency so as to reduce the required efficacious dose/exposure. First, we evaluated several novel fused heteroaromatic in place of the pyrazolopyrazine moiety as right-hand side. Gratifyingly, the use of an imidazopyridazine fragment led to a potency increase of roughly 10-fold providing us with a novel and promising subclass (Figure 2, compounds **4** and **5** as compared to

DOI: 10.1021/acs.jmedchem.8b00741
J. Med. Chem. XXXX, XXX, XXX−XXX

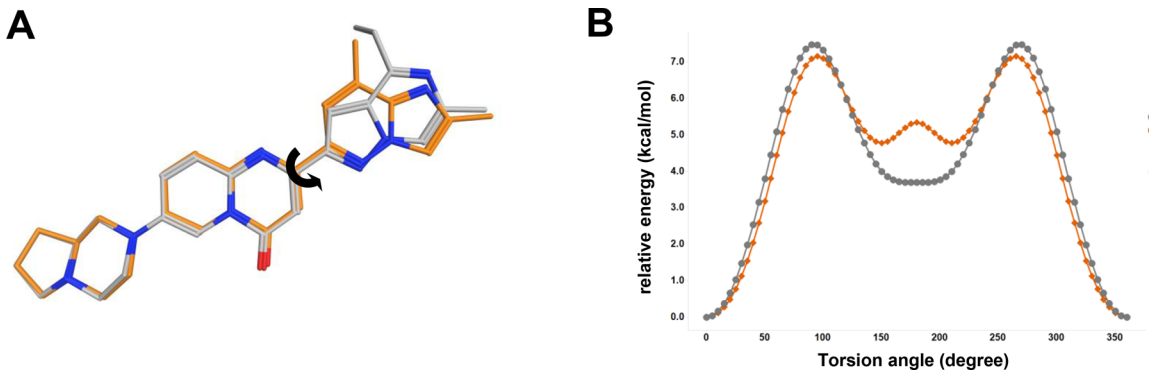

Figure 3. Structural overlay (A) and gas phase QM torsional angle scan statistics for the indicated bond (B) for compound **3** in gray and compound **4** in orange.

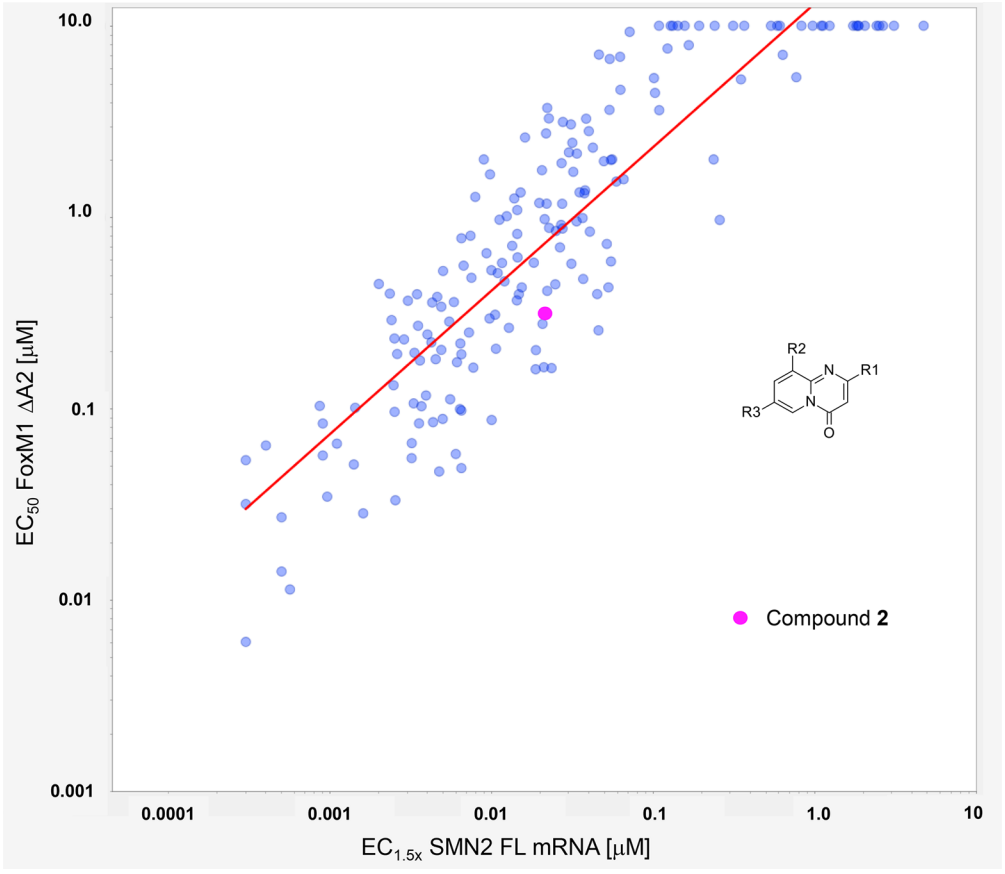

Figure 4. The potency of compounds in the pyridopyrimidinone series in modifying the splicing of *SMN2* exon 7 and *FOXM1* exon A2 is correlated.

compound **3**). Compound **3** contains the same pyrazolopyrazine moiety as compound **2**.[9]

The novel imidazopyridazine fragment conserved the conformational preorganization and planarity of the right-hand side which has been shown previously to be crucial to obtain potent compounds (Figure 3). SAR analysis indicates that the pyrazine nitrogen provides an important molecular interaction and is critical for a high in vitro potency. The change of the hydrogen-bond binding energy in imidazopyridazine fragment contained in compounds **4** and **5** relative to pyrazolopyrazine from compound **3** (−8.06 kcal/mol vs −7.16 kcal/mol respectively estimated by QM) could contribute to the observed increase in potency.

Next, to establish a structure−activity relationship (SAR) for *FOXM1* splicing in order to further increase selectivity in favor of *SMN2* splicing, we tested an already existing pool of 210 derivatives from the pyridopyrimidinone series for their activity in *FOXM1* splicing assay. A clear correlation (Figure 4, red line, regression analysis) was observed between the in vitro splicing activity of *SMN2* ($EC_{1.5x}$ FL mRNA in HEK293H) and *FOXM1* (IC_{50} ΔA2 in fibroblast). Compounds were generally 10-fold more potent against SMN2 than FOXM1. However, compound-mediated modulation of *SMN2* and *FOXM1* alternative splicing appear mechanistically related so that substantially increasing the in vitro selectivity for *SMN2* over *FOXM1* appeared not to be feasible.

DOI: 10.1021/acs.jmedchem.8b00741
J. Med. Chem. XXXX, XXX, XXX−XXX

We therefore adapted our optimization strategy and focused on an increase of the in vivo selectivity between *SMN2* and *FOXM1* splicing as an improvement versus compound **2**. We found that compound **2** can be metabolized in vitro to form N-dealkylated metabolite **6** across all species tested (human, rat, dog, minipig, cynomolgus monkey, mouse, and rabbit; Figure 5). Upon oral administration in rodents and cynomolgus

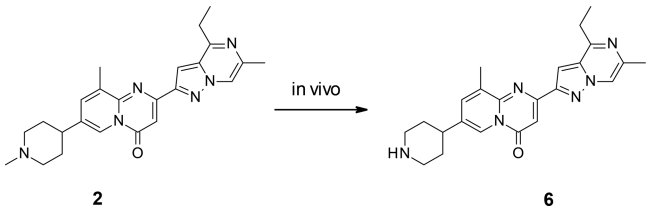

Figure 5. In vitro and in vivo metabolism of **2** leading to **6**.

monkeys, we observed the formation of this metabolite **6** with plasma concentrations reaching up to 9% of those for parent compound **2**.

Metabolite **6** is 10-fold more potent than parent compound **2** in vitro in SMA patient-derived fibroblasts in both *SMN2* ($EC_{1.5\times}$, SMN FL = 2 nM) and *FOXM1* (EC_{50}, FOXM1, ΔA2 = 23 nM) splicing assays. The higher potency of the metabolite was also observed on *FOXM1* mRNA expression levels in human and cynomolgus monkey iPSCs with an IC_{50} of 119 nM and 103 nM, respectively. However, metabolite **6** was found to be a strong P-gp substrate with an efflux ratio (ER, a measure of P-gp-mediated efflux) of 18.7 in human and 20.0 in mouse cells. Therefore, not surprisingly, metabolite **6** did not elicit SMN protein increase in brain but only in muscles of adult C/C-allele mice, a mouse model of mild SMA[15] when dosed orally once daily for 10 days, despite the high drug levels in plasma. Therefore, being peripherally restricted, metabolite **6** can contribute to potential side effects mediated by the induced *FOXM1* isoforms in peripheral organs and tissues but not contribute to the CNS activity in term of SMN protein increase. Hence, part of our revised strategy to improve the therapeutic window in vivo was to avoid formation of peripherally restricted active metabolites. Thereby, the peripheral side effects induced by *FOXM1* splicing could be minimized.

We evaluated two approaches to suppress the N-dealkylation: (1) making the *N*-alkyl residue a part of a ring or (2) moving the alkyl residue to an adjacent location (Figure 6).

At this stage, the central core (the pyridopyrimidinone moiety) and the right-hand-side fragment (a novel imidazo-pyridazine moiety) had been fixed. We knew that a very large diversity of amine fragments is tolerated on the left as long as it contains a basic amine with a pK_a above 6.5 (to maintain in vitro potency). To define the optimal amine moiety, we considered several additional molecular properties descriptors. One of them was the lipophilicity of the final molecule. We have previously shown that lipophilicity in this series was a strong predictor of the P-gp efflux. Therefore, we continued designing molecules with a calculated lipophilicity between 1.6 and 3.0 to achieve respectively a human P-gp ER below 2.5 and to prevent a high clearance and nonspecific protein binding.[16]

The hERG affinity and phospholipidosis (seen with compound **2**) can generally be reduced by the lowering of the basicity of an amine present in the molecule. In addition, we had determined that volume of distribution of compounds in this series (e.g., compound **2** V_{ss} is around 20−30 L/kg in cynomolgus monkeys and rodents) is correlated with the basicity of the molecule (Table 1, Figure 7). We had to strike an optimal balance between basicity and lipophilicity while maintaining potency. We focused on selecting a left-hand-side basic amine moiety with the lowest bpKa (but still above 6.5).

Taking into consideration those criteria, we prepared a virtual library of final compounds containing amines, with a calculated log *D* between 1.6 and 3 and a calculated basic pK_a between 6.5 and 8 (the lower the better) and not subject to N-dealkylation (Figure 8). The amine fragments were selected by a matched pair analysis from in house molecules.

This exercise led us to a list of roughly 100 virtual compounds. After a visual inspection of the chemical structure to remove any amine fragments with unwanted features (reactive or unstable functional groups for example), we identified 40 compounds of interest which were prepared and characterized. Compound **1** came out on top due to a combination of very high potency, strongly reduced basicity, no phototoxicity risk, and the lack of active metabolites (Figure 9).

Preclinical Characterization of 1. Compound **1** was subjected to a full characterization. It displayed an improved and very high in vitro potency on *SMN2* splicing, while the basicity has been drastically reduced by nearly 4 log units (Table 2). The lipophilicity was maintained to 2.5; hence compound **1** was not a human P-gp substrate. Fraction unbound in plasma was around 10% and similar across species.

Compound **1** was active in vitro in SMA patient-derived fibroblasts and in motor neurons generated from induced pluripotent stem cells (iPSCs) derived from SMA type 1 patient fibroblasts, promoting the inclusion of exon 7, to generate full-length (FL) mRNA. SMN protein levels were also increased (Figure 10).

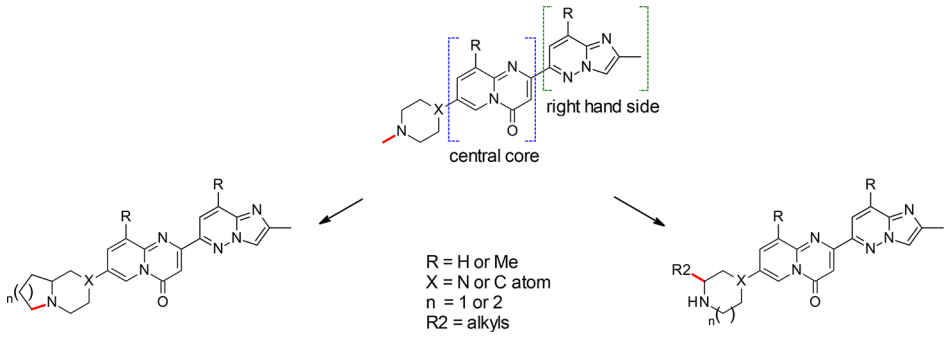

Figure 6. Two approaches to suppress the formation of N-dealkylated active metabolites.

DOI: 10.1021/acs.jmedchem.8b00741
J. Med. Chem. XXXX, XXX, XXX−XXX

Table 1. Volume of Distribution Measured in Rat and pKa

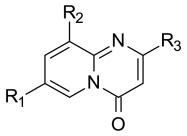

Compd	R^1	R^2	R^3	*c*pKa	*m*pKa	Vss (L/kg)
2		Me		8.8	10.9	29
7		H		7.9	7.6	7
8		H		8.2	8.4	15
9		H		8.3	7.7	10
10		Me		9.0	9.1	20
11		H		9.6	8.9	20
12		H		8.6	8.6	15
13		H		7.7	7.2	5
14		H		8.0	7.3	7
15		H		8.2	8.4	9
16		H		9.9	9.3	18
17		H		7.9	7.5	4

In vitro metabolism studies using human liver microsomes and human hepatocytes identified N-hydroxylated derivative **18** (Figure 11) as the main metabolite (although formed at a low level of 3.8% and 1.7%, respectively). Compound **18** was assessed for its potency on both *SMN2* and *FOXM1* splicing assays and was inactive as anticipated (due to removal of basicity).

This was confirmed by assessing the effect of compound **1** and its metabolite **18** on the expression level of *FOXM1* mRNA variants (*FOXM1b/c*) in human and cynomolgus monkey induced pluripotent stem cells (iPSCs). While **1** modified *FOXM1* splicing with IC_{50}, ΔA2 of 113 nM and 155 nM respectively, its metabolite **18** did not show any effect. This is in sharp contrast to the compound **2** and its metabolite **6** and met our design criteria.

A favorable drug metabolism and pharmacokinetic (DMPK) profile in the rat and cynomolgus monkey was observed for **1** upon intravenous and oral administration (Table 3). Noteworthy, the volume of distribution 3.1 L/kg (rat) and 2.0 L/kg (cynomolgus monkey) is markedly reduced compared to our first compound **2**. This outcome is perfectly in line with the marked basicity reduction of the compound **1** (mpKa of 6.8) as initially hypothesized. Furthermore, the half-life of the compound was also markedly reduced being in a more favorable range of 5−6 h upon oral administration.

Preclinical Efficacy of 1. We then evaluated compound **1** in two mouse models of SMA. Adult C/C-allele mice with mild SMA phenotype were treated for 10 days with compound **1** given once a day orally at three different doses (1, 3, and 10 mg/kg). The level of SMN protein was assessed in brain and in quadriceps muscle (Table 4). In the Δ7 mouse model of severe SMA,[17] compound **1** was administered by intraperitoneal (ip) injection once daily starting on postnatal day (PND) 3 and continued through PND9. The level of SMN protein was assessed in brain and in quadriceps muscle as well (Table 5). A maximum SMN protein increase was already reached at 1 mg/kg (free AUC_{0-24h} extrapolated from 3 mg/kg exposure = 73 ng.h/ml), whereas a dose of 3 mg/kg (free AUC_{0-24h} = 118 ng.h/ml) for compound **2** led to a lower SMN protein increase. These data demonstrate that **1** potently increases SMN protein in both brain and muscle tissues of transgenic mouse models of SMA.

The impact on the lifespan and body weight of Δ7 SMA mice treated with compound **1** was also assessed daily (Figure 12). During the observation period, only two heterozygous littermates died. In contrast, all vehicle-treated mice died before PND21 with a median survival time (MST) of 10.5 days. Compound **1** treatment prolonged animal survival at all doses, with a minor but significant effect already at the lowest dose tested (MST of 26 days), whereas for the other dose groups minimal differences from heterozygous littermates were observed. Body weight gain followed a similar trend. These data indicate that treatment with compound **1** prevents the manifestation of the SMA phenotype in the severely affected Δ7 SMA mice when dosing is started at PND3.

Finally, we evaluated the effect of compound **1** on neuromuscular pathology in the Δ7 SMA mouse model. Animals were treated from PND3 to PND14 by ip administration of vehicle or compound **1** at doses of 0.1, 0.3, and 1 mg kg^{-1} day^{-1}. Spinal cord and muscle tissues were processed for histological assessment. Relative to heterozygous littermates, SMAΔ7 mice showed a significant loss of vesicular glutamate transporter 1 (vGlut1)-positive proprioceptive inputs onto motor neuron, loss of motor neurons, neuromuscular junction (NMJ) denervation in the longissimus muscle, and muscle atrophy. Upon treatment with compound **1**, we observed a significant and dose-dependent increase of number of vGlut1 inputs, the number of motor neurons, the percentage of fully innervated NMJs and increased muscle size in the extensor digitorum longus (EDL) muscles relative to those in vehicle-treated SMNΔ7 mice (Figure 13).

Nonclinical Safety of 1. Compound **1** was also subjected to preclinical safety assessment. The effect on the hERG channel was assessed at 37 °C. No effect on the hERG K^+ current was observed (IC_{20} > 5 μM). This marked improvement compared to compound **2** can be attributed to the strongly reduced basicity of the molecule. A telemetry study was performed in cynomolgus monkey which confirmed the absence of QTC interval prolongation as well as absence of any other cardiovascular findings.

In an in vitro phototoxicity assessment using the standard neutral red uptake in 3T3 fibroblasts assay, the compound did not show any effect up to the highest solubility-limited concentration of 9 μM (~3600 ng/mL), i.e., well above any expected therapeutic free concentration. This improvement is

DOI: 10.1021/acs.jmedchem.8b00741
J. Med. Chem. XXXX, XXX, XXX−XXX

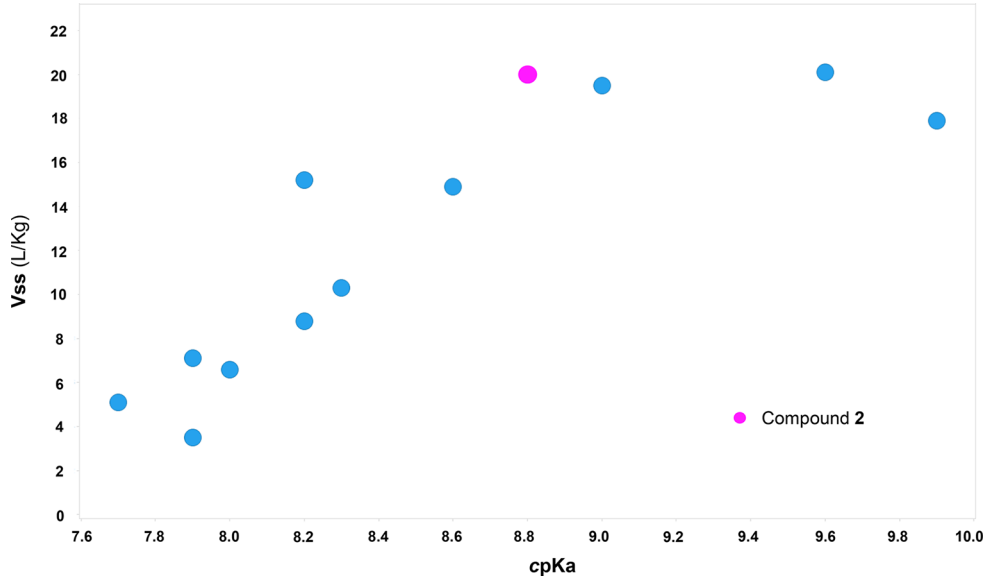

Figure 7. Volume of distribution (V_{ss}) measured in rat versus calculated basicity (cpKa).

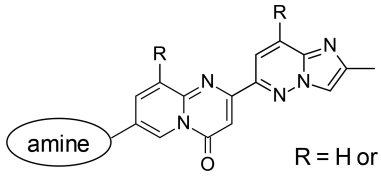

Figure 8. Virtual library to define compounds with optimal combination of basicity, lipophilicity, and potency.

Table 2. In Vitro Potency and Physicochemical Characterization

compd	SMN2 splicing $EC_{1.5\times}$ [nM]	FOXM1 splicing EC_{50} [nM]	SMN protein $EC_{1.5\times}$ [nM]	log *D*	h P-gp ER	mp*Ka*	f_{u_p} [%] h/m
1	4	67	29	2.5	2.2	6.8	11/10
2	23	247	87	2.3	2.0	10.9	13/2

most likely due to the use of the novel right-hand-side fragment (the imidazopyridazine).

No evidence of phospholipidosis has been observed in vivo in nonclinical safety studies which again can be attributed to the reduced basicity (4 units lower), reduced calculated amphiphilicity, reduced volume of distribution (from 20 to 2 L/kg), and an improved potency (leading to lower efficacious AUC). Specifically, compound **1** did not display any evidence for phospholipidosis in any tissues, at the doses tested, when administered chronically with daily oral gavage for up to 26 weeks to rats or up to 39 weeks to cynomolgus monkeys up to the highest doses tested.

Role of Selectivity in Safety. In a comprehensive strategy to profile fully compounds **1** and **2** for their effects on pre-mRNA splicing in general, the safety assessment strategy included a genome-wide splice site analysis, which identified a potential of compounds **1** and **2** to engage splice sites beyond the SMN2 target. Results of this analysis and specific functions of gene splice variants associated with it were compared with the observations made in the repeat dose animal toxicity studies with compounds **1** and **2**. The selected animal species for these studies have been rats and cynomolgus monkeys based on their well-known characterization in toxicity studies for small molecules while acknowledging at the same time that *SMN2* gene is unique to humans and absent in the commonly used animal species in toxicity testing. Hence, toxicities seen in animals with compounds **1** and **2** were either characterized as unrelated to its action on pre-mRNA splicing (off-target) or as related to the compound interactions with the splicing machinery but affecting splicing targets other than *SMN2* (termed secondary targets). Yet, similar to their quick onset of action on the *SMN2* target in vitro and in transgenic mice, the results of engagement of secondary splice targets in *SMN2* nonresponder animals became visible soon after start of repeat dose toxicity studies and did not change much in severity with chronic dosing. Findings of toxicological significance for compound **1** (as with compound **2**) were observed mainly in organs with rapid cell turnover in mice, rats, and cynomolgus monkeys. Looking into the range of secondary splice targets

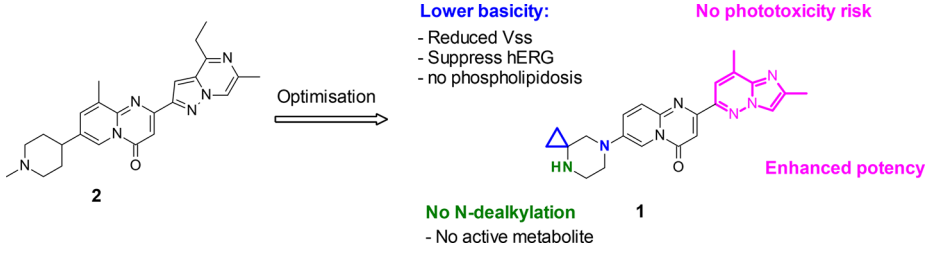

Figure 9. Optimization from **2** leading to the discovery of **1**.

DOI: 10.1021/acs.jmedchem.8b00741
J. Med. Chem. XXXX, XXX, XXX−XXX

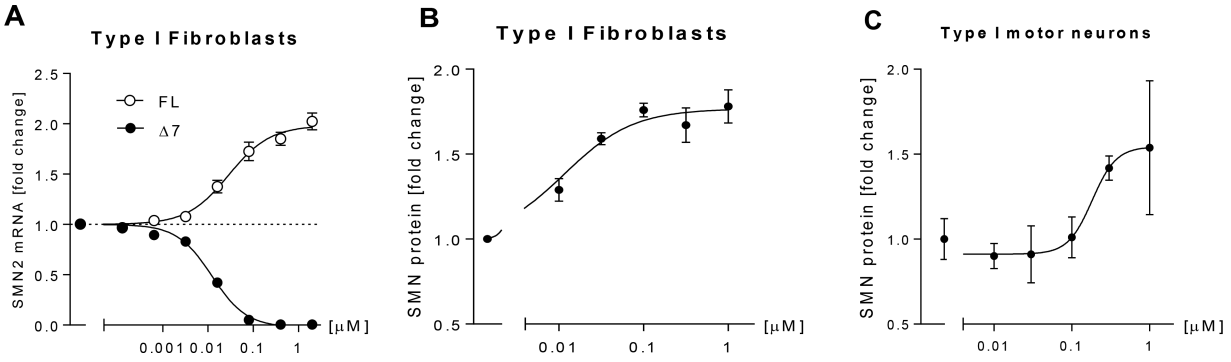

Figure 10. Compound **1** tested in (A) SMN2 splicing in SMA type I fibroblasts, (B) SMN protein in SMA type I fibroblasts, and (C) SMN protein in SMA type I motor neurons. FL = full length, and Δ7 = mRNA lacking exon 7.

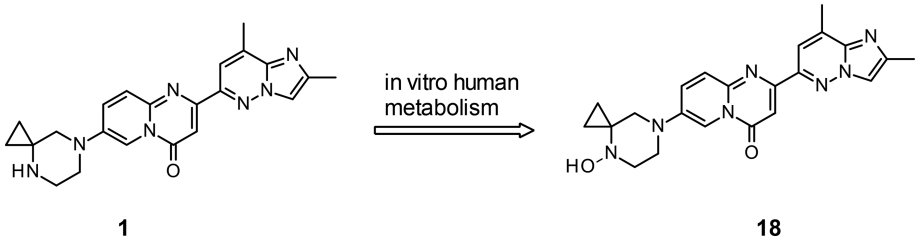

Figure 11. In vitro metabolism of **1**.

Table 3. In Vivo Single-Dose Pharmacokinetic (SDPK) Profile for Compounds 1 and 2[a]

	rat				cynomolgus monkey			
compd	Cl[a] (mL min^{-1} kg^{-1})	V_{ss}[a] (L/kg)	$T_{1/2}$[b] (h)	F[b] (%)	Cl[c] (mL min^{-1} kg^{-1})	V_{ss}[c] (L/kg)	$T_{1/2}$[d] (h)	F[d] (%)
1	8.9	3.1	6.4	~100	5.7	2.0	5.4	43
2	25	29	19	~100	5	20	42	52

[a]For compound **1**: (a) iv, 1.9 mg/kg; (b) po, 5.5 mg/kg; (c) iv, 0.1 mg/kg; (d) po, 0.5 mg/kg. For compound **2**: (a) iv, 2 mg/kg; (b) po, 5 mg/kg; (c) iv, 0.3 mg/kg; (d) po, 1.3 mg/kg.

Table 4. Pharmacokinetics and SMN Induction in Adult C/C-Allele Mouse Model

compd	dose (mg/kg po)	total plasma[a] AUC_{0-24h} (μg·h/mL)	% SMN increase in brain	% SMN increase in quadriceps
vehicle	0	0	0	0
1	1	na[b]	0	0
1	3	na[b]	17	0
1	10	9.0	100	49

[a]Plasma AUC determined in a satellite group. [b]Not assessed.

Table 5. Pharmacokinetics and SMN Induction in Neonatal Δ7 Mouse Model

compd	dose (mg/kg ip)	total plasma[a] AUC_{0-24h} (μg·h/mL)	% SMN increase in brain	% SMN increase in quadriceps
vehicle	0	0	0	0
1	0.1	na[b]	28	32
1	0.3	na[b]	90	64
1	1	na[b]	206	210
1	3	2.2	202	241

[a]Plasma AUC determined in a satellite group of neonatal (P10) wild-type mice. [b]Not assessed.

identified with the genome-wide splice-site analysis, these phenotypes of toxicity observed in the toxicity studies above the no observed adverse effect level (NOAEL) are in line with an effect of this compound on genes such as *FOXM1* and/or *MADD*, i.e., genes the functions of which are associated with cell cycle and apoptosis processes and for which splice variant changes result in changes in function. The findings were reversible or partially reversible in nature (depending on the chosen reversibility period and cell turnover in the respective organs) and included the following:

- micronucleation (MN) induction in vitro in mouse cell lines and in rat bone marrow erythroblasts and decreased cellularity in bone marrow;
- histopathological changes in gastrointestinal tract epithelia (increased apoptosis/single cell necrosis) and lamina propria (vacuolation) and exocrine pancreas epithelia (single cell necrosis) in mice, rats, and/or cynomolgus monkeys;
- parakeratosis/hyperplasia/degeneration of the skin, tongue, and larynx epithelia with associated inflammation in cynomolgus monkeys;
- degeneration of germ cells in the testis of cynomolgus monkeys and rats.

Most importantly for clinical evaluation of safety and efficacy of compound **1**, the in vitro and animal toxicity studies with compound **1** yielded clearly no observed adverse effect levels (NOAELs) for all of the findings listed above. Consistent with the hypothesis of a transient effect on splice variants, adverse effects were reversible upon cessation of treatment. Consistent with the approach to improve potency, adverse effects were only

DOI: 10.1021/acs.jmedchem.8b00741
J. Med. Chem. XXXX, XXX, XXX−XXX

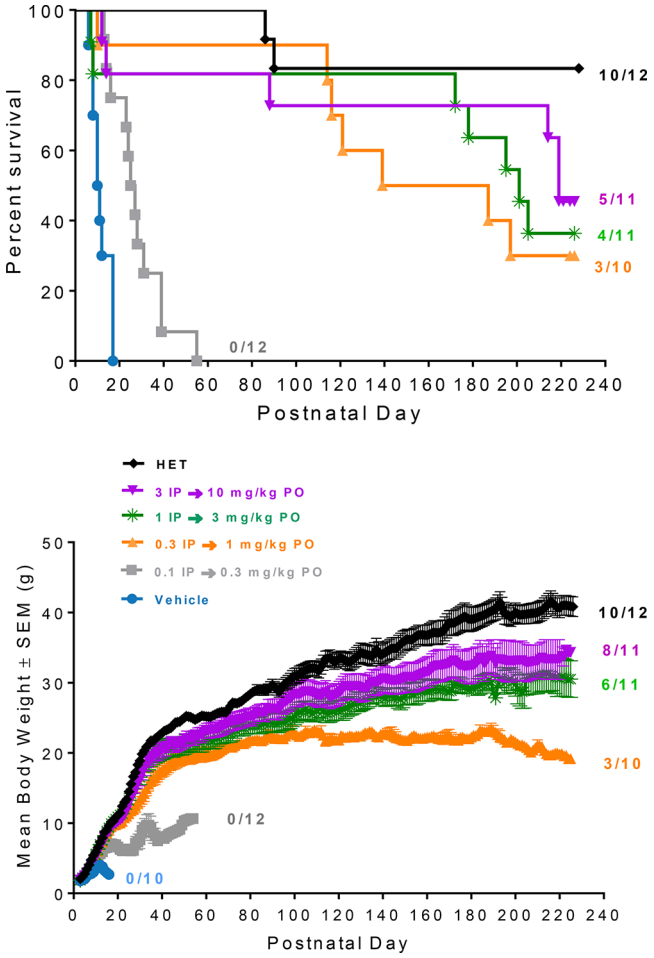

Figure 12. Survival and body weight gain of Δ7 mice treated with compound **1**. Animals were treated once daily with vehicle or compound at doses of 0.1, 0.3, 1, and 3 mg kg^{-1} day^{-1} from PND3 to PND23 by ip injection and thereafter by oral gavage at doses of 0.3, 1, 3, and 10 mg kg^{-1} day^{-1}.

observed at exposures significantly above exposures predicted to be associated with the desired degree of modification of *SMN2* pre-mRNA splicing and SMN protein increase in SMA patients. Thus, the overall clear NOAEL for adverse effects seen in animals enabled the identification of efficacious exposures for compound **1** which could be safely tested in healthy volunteers and in SMA patients while still maintaining a full pharmacodynamic response. The findings also identified with reliability safety parameters that can be monitored in human clinical trials with compound **1** in the unexpected case of a higher sensitivity of humans as compared to animals used for toxicological evaluation. The currently available clinical evidence for safety and pharmacodynamic response of compound **1** supports this strategy.

To determine possible mechanisms behind these animal toxicities and their relevance to humans, compounds **1** and **2** and a series of earlier *SMN2* splice modifiers were tested for their specificity of interaction with the splicing machinery.[11] These included primary and secondary splice target investigations in (1) patient cells, (2) induced pluripotent stem cells from human and cynomolgus monkey, (3) cells of tissues of rats and cynomolgus monkeys affected with the observed toxicities (compared with the reference organ spleen, which was selected based on absence of major toxicities but easily amenable to analysis for its relatively homogeneous cell population). Figure 14 shows the effects of compounds **1**, **2**, and **6** and branaplam on the splicing of the primary target *SMN2* and on the most pronounced secondary splice targets (of either compound, note the differences in specificity). This is based on in vitro experiments with SMA patient-derived fibroblasts at concentrations active on SMN2 splicing; thus different concentrations of the respective compounds were used. Most prominent secondary splice targets in these experiments were *STRN3*, *FOXM1*, *MADD*, *APLP2*, and *SLC25A17* mRNAs.

In summary, compounds **1** and **2** do indeed show good selectivity toward the *SMN2* target, with most of the secondary splice target effects seen with very weak or even undetectable levels at the concentrations with full pharmacodynamics effect on the SMN2 target.

The splicing events described cover a range of biological effects.

For *SMN2*, exon 7 inclusion is promoted, leading to the desired increased production of a functional full length SMN protein. In the animal experiments in vitro or in vivo, no changes in SMN splicing could be observed with compound **1** or **2** due to the lack of *SMN2* gene and divergent 5′ splice site in *Smn1*.

For *STRN3*, targeting of a donor site in all species (mice, rats, cynomolgus monkeys, and humans) leads to the production of an at best rare, maybe nonphysiological protein variant that includes only one of two exons that usually come together. However, the event will "only" introduce an additional 37 amino acids into the protein and may not abolish the protein completely. It remains unclear whether there could be any safety issue stemming from changes in *STRN3* splice variants as there is little evidence from the published literature which would be compatible with the phenotypes seen in toxicity studies.

For *FOXM1*, the increased use of two different 5′ splice sites in the same exon can play a role. The annotated donor splice site can lead to the formation of a dominant-negative form of the protein, whereas use of a cryptic internal donor site results in the production of the C terminus-truncated FOXM1ΔC isoform which has been observed in several cancer cell lines[12] . FOXM1ΔCis a dominant negative inhibitor of wild type FOXM1 function as a transcriptional factor and has been shown to interfere with normal cell cycle progression, induce chromosome instability and aneuploidy. Changes in FOXM1 with formation of a dominant negative exon inclusion form, which inhibits cell cycle progression, were seen in cynomolgus monkey cells and tissues. In the rat *Foxm1* gene the region encoding exon A2 is absent, and therefore, these splice variants cannot form but an overall reduction of FoxM1 expression was observed when rodent cells used for the in vitro micronucleus test were analyzed for effects on Fox M1. On the basis of the known involvement of FOXM1 in cell cycle progression, changes in its splice variants may be the most important factor for understanding of the toxicities observed in particular in cynomolgus monkeys with compounds **1** and **2** and other SMN2 splice modifiers.

For *APLP2* and *MADD*, rare but physiologically relevant exons are included at an increased rate, modulating the protein function in ways that are not fully understood. However, clear changes in the splice variants of *MADD* were also seen in cells and tissues from rats and monkeys treated with compounds **1** and **2**. One of the known splice variants of *MADD*, IG20, was upregulated in tissues or rats and cynomolgus monkeys, in which apoptosis was seen. IG20 is described as a proapoptotic splice variant of MADD.

DOI: 10.1021/acs.jmedchem.8b00741
J. Med. Chem. XXXX, XXX, XXX−XXX

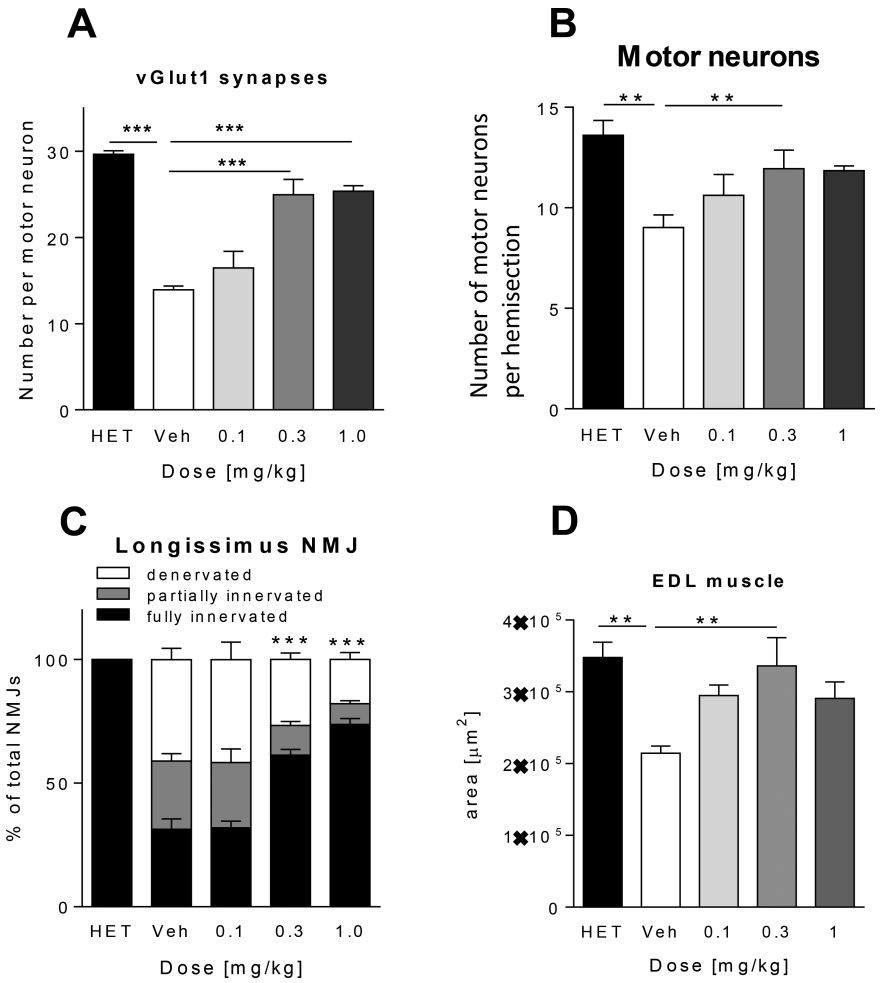

Figure 13. Δ7 SMA mice treated with **1** from PND3 to PND14. Neuromuscular connectivity and muscle atrophy were assessed by immunohistochemistry. (A) vGlut1-positive proprioceptive inputs in L3−5 spinal cord. (B) Ventral motor neurons in L3−5 spinal cord. (C) NMJ innervation onto longissimus muscle. (D) EDL muscle cross-sectional area. ∗ = $p < 0.05$; ∗∗ = $p < 0.01$; ∗∗∗ = $p < 0.001$ vs vehicle-treated mice.

Finally, for *SLC25A17*, inclusion of exon 3 was observed and in a small fraction of products a downstream cryptic 5′ splice site was also activated. According to the current genome assignment, exon 3 encodes an alternative translation start codon predicted to generate SLC25A17 protein with an alternative N-terminus.

To elucidate the mechanism of micronucleus (MN) formation and/or exclude direct DNA reactivity, a number of in vitro and in vivo studies were performed using known methodologies.[20] No induction of γH2AX, a biomarker for DNA double-stranded breaks, was observed at concentrations compatible with cell survival in L5178Y mouse lymphoma cells or TK6 human lymphoblastoid cells. The proportion of apoptotic cells was increased at cytotoxic concentrations, but cell cycle perturbations or relevant responses in other in vitro end points like phosphorylation of histone H3 or polyploidy were not observed. Acute treatment of rats over 3 days with up to 25 mg kg^{-1} d^{-1} in a combined MN/comet study did not induce primary DNA-damage as measured with the comet assay in liver while a clear, dose-dependent increase of the frequency of micronucleated erythrocytes was observed. A conclusive mechanism for the induction of micronuclei by compound **1** could not be demonstrated, but the evidence described above strongly points toward an indirect mode of action (e.g., related to secondary splice target interaction) and excludes direct DNA-reactivity. Therefore, a linear dose−response relationship must not be assumed but rather a sublinear, "threshold-type" curve should be used to derive appropriate safety margins. On the basis of the most recent recommendations of the International Workshop on Genotoxicity Testing (IWGT),[21] the benchmark-dose (BMD) concept was applied to determine the point-of-departure (PoD) with the software PROAST[22] using Hill modeling. The variability of solvent control samples (i.e., the "background noise") of the micronucleus assays suggests a critical effect size (CES) of approximately 50% to calculate the benchmark-dose lower confidence limit (BMDL, equivalent to the critical effect dose lower confidence limit CEDL) of exposure to compound **1** for micronucleus induction.[23] Studies performed with young (QD 13 week treatment duration) and adult (both acute 2 days and QD 4 week treatment duration) rats were used to derive C_{max} and AUC_{0-24h} values for compound **1** that would not lead to relevant increases of micronucleated erythrocyte frequencies. Graphical representations of the modeling are shown Figure 15.

Other Types of Toxicities Observed in Animals Treated with Compounds 1 and 2. In addition to the above-mentioned findings in animal toxicity studies, histological findings were present in the retina of cynomolgus monkeys. These were noted with chronic daily oral treatment for both compounds **1** and **2**. Retinal degeneration was observed during and at the end of daily oral dosing for 39 weeks. During the in-life

DOI: 10.1021/acs.jmedchem.8b00741
J. Med. Chem. XXXX, XXX, XXX−XXX

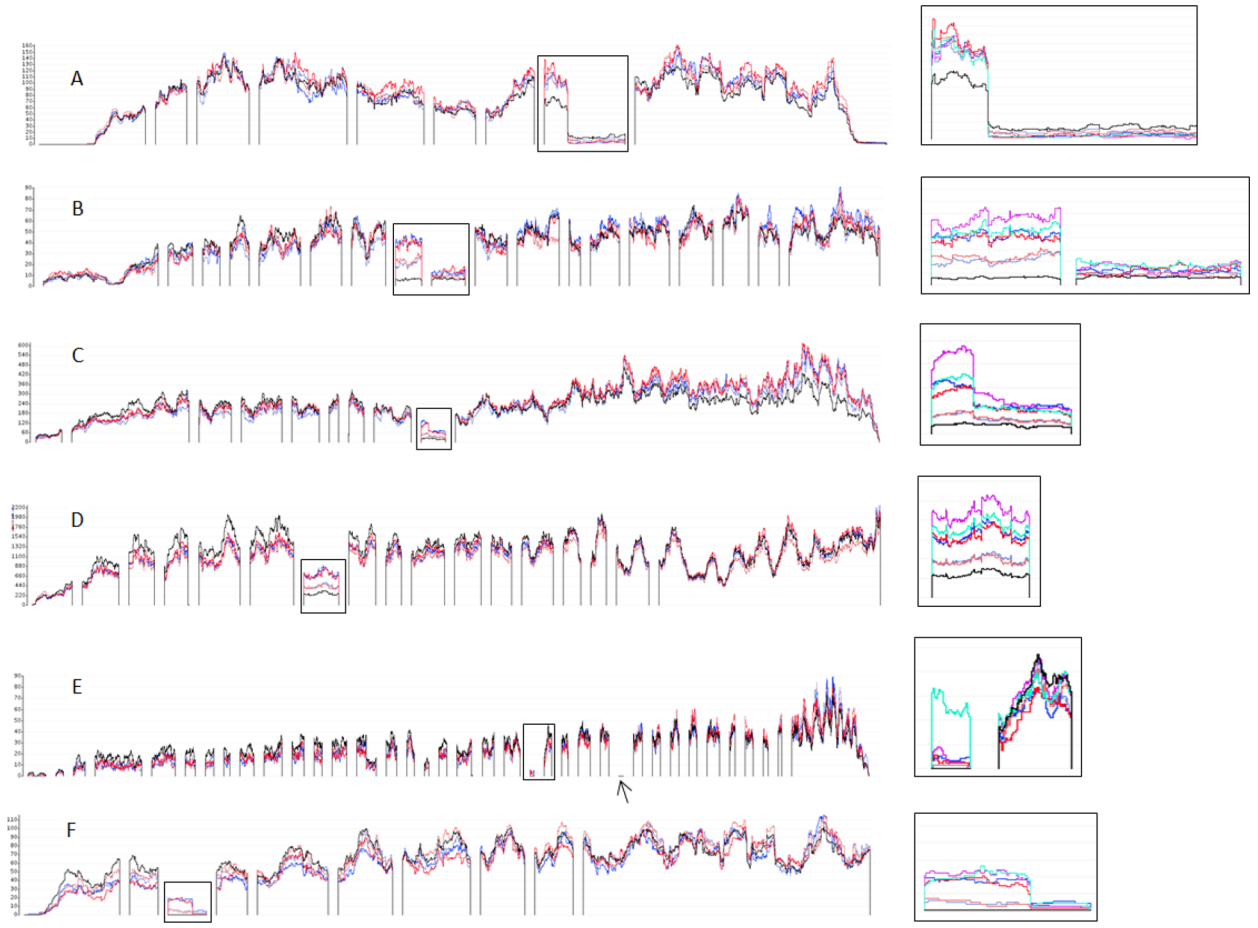

Figure 14. Splicing effects on target and selected off-target transcripts. The diagrams show numbers of reads mapped to six human genomic loci in various conditions. Each peak corresponds to an exon present in mature mRNA. Note that exons and introns are not drawn to scale, and lengths of loci differ substantially. The diagrams on the left present complete overviews of the loci, and a detailed view of the critical region (affected by at least one of the compounds tested) is shown enlarged on the right. Black: vehicle-treated control samples (human patient fibroblasts). Red: 131 nM (light) and 655 nM (dark) doses, respectively, of compound **2**. Blue: 121 nM (light) and 605 nM (dark) doses, respectively, of compound **1**. For the detailed views on the right, also added are compound **6**, the potent metabolite of compound **2** (at 95 nM, in magenta), and branaplam, at 24 nM (cyan). (A) *SMN2*. All compounds show very comparable on-target effects. For compounds **2**, **6**, and **1**, increasing the doses to higher values did not have any marked additional effect on the on-target activity, indicating a saturation of the on-target effect. The 3′-most part of the exon is higher in controls and repressed by all the treatments, consistent with a switch between the spliced and read-through forms. (B) *STRN3*. Next to *SMN2*, striatin 3 splicing is most consistently affected by all compounds tested, probably due to a very similar splicing mechanism.[11] For this gene, two variants are well described that either include or exclude two adjacent exons, exons 8 and 9 (highlighted). In the control samples (black), both exons are present at similarly low levels, indicating that they are skipped in the majority of transcripts. As shown in the right panel, all the tested compounds have a rather specific splicing effect on only the first of the two, exon 8, to produce a splice variant that was described earlier but is not well characterized and that does not appear to play any major role under physiological conditions. Compounds **2** and **1** at lower doses have minor effects on *STRN3* exon8 (left) that however increase dose dependently. In comparison, exon 9 (right) is affected to a much lower degree. Both compound **6** and branaplam have effects comparable to the higher doses of compounds **2** and **1** (and about twice as high as for the lower doses of compounds **2** and **1**), indicating some selectivity for both compounds toward the on-target, *SMN2*. Exon 8 has a length of 111 bp, divisible by 3, so inclusion of this exon alone does not interrupt the *STRN3* open reading frame (exon 9 is 141 bp long, again an "in-frame" exon). (C) *FOXM1* is a key cell cycle regulator and, as such, potentially critical for off-target effects. The affected splicing event, at first glance, is the inclusion or exclusion of exon A2 (also referred to as exon VIIa or exon 9) that disrupts a protein domain of *FOXM1*, leading to a dominant-negative variant of the protein that retains the ability to bind DNA but lacks the transactivation domain and therefore cannot promote DNA transcription.[18] This domain is usually not included, or only at very low levels, in controls (black line). Compounds **2** and **1** at their lower concentrations have a very moderate effect on inclusion of the complete exon A2. In addition, compounds **6** and branaplam and compounds **2** and **1** at their higher doses appear to activate, to a much higher degree, an alternative 5′ splice site located inside exon A2 leading to the generation of the *FOXM1*ΔC isoform that has been previously described.[12] This isoform contains only the first 34 nucleotides of exon A2 resulting in a frameshift and the generation of the truncated FOXM1ΔCprotein. (D) *APLP2* is another pre-mRNA whose splicing was found to be affected by various compounds, albeit very weakly by the low doses of compounds **1** and **2**. The affected exon is 168 bp long (no change in the reading frame) and is used in about one-quarter of the total transcripts in controls. Compounds **6** and branaplam increased the usage of this exon by more than 2-fold in this experiment, whereas compounds **2** and **1** have slightly lower effects even at their higher doses. (E) *MADD* has a complex gene structure with many exons and various splice variants described, most of which are not fully annotated or characterized. The affected exon here is absent in controls, as shown in the panel on the right (the neighboring exon to the right is included for reference in the detailed view). The black arrow points to another facultative exon that is coexpressed with the boxed exon in all annotated variants of this gene. As for several examples above, compounds **2** and **1**, at their lower concentrations, have only a very small effect on this exon. Compound **6** at the dose used here and compounds **2** and **1** at their higher doses show somewhat stronger effects that are, however, still very weak. In contrast, branaplam leads to an almost complete inclusion of the exon into all MADD transcripts. The second exon (arrow) does not appear to be affected by any of the compounds and always remains very low or absent. (F)

DOI: 10.1021/acs.jmedchem.8b00741
J. Med. Chem. XXXX, XXX, XXX−XXX

Figure 14. continued

SLC25A17. Exon 3 comes in two forms of different lengths. The shorter, canonical form of the exon (5′ part) is not included in controls but is very weakly affected by compounds **2** and **1** at their lower doses. At higher doses, and for branaplam, this exon is included in about 50% of all *SLC25A17* transcripts. There is a very weak effect of all compounds on an extended, noncanonical form of this exon. These graphs were generated using the software Manananggal.[19]

phase, multifocal peripheral retina degeneration in the photoreceptor layer and microcystic spaces in the inner retinal layers were detected using optical coherence tomography (OCT). This was associated with a depressed B-wave which was more obvious in a scotopic (rod-driven) than a photopic (cone-driven) light setting in the electroretinogram (ERG). Histologically, the most affected layers were the outer nuclear layer (ONL) and photoreceptor layer with additional vacuolation of the inner nuclear layer (INL). Incidence and severity of the findings were dose dependent, and the changes were located mostly in the periphery. A no observed effect level (NOEL) for the retinal findings was established. In a 22 week recovery phase after 39 weeks of treatment, retinal degeneration with peripheral photoreceptor loss remained present. However, as observed using OCT, microcystic macular degeneration decreased significantly and areas of white speckled hyperfluorescence became less dense. In previously treated animals, ERG amplitudes noticeably increased by the end of the recovery phase showing normal ERGs in 3 out of 4 animals. Histologically, retinal degeneration with photoreceptor loss and retinal pigment epithelium (RPE) hypertrophy were still present, but the vacuolation of the INL had reversed which can explain the recovery from depressed ERG responses. Experimental evidence suggested that the effect on the retina is not directly associated with effects on tissue proliferation but related to high melanin binding observed in vitro, to tissue retention in the retina, and impairment of lysosomal/autophagosomal function in retinal pigmented epithelial cells. For compounds **1** and **2**, similar NOELs were established for these retinal changes in chronic dosing studies in cynomolgus monkeys. As retinal changes were seen with both compounds, they could potentially represent a class effect of this series of *SMN2* splice modifiers, which are independent of their action on the spliceosome. This was followed up with investigation of both compounds with chronic treatment in pigmented rats versus albino rats. Similar to pronounced accumulation with repeated dosing in melanin-containing retinal tissue in monkeys, we have found pronounced accumulation of compounds **1** and **2** in these retinal tissues in pigmented rats but not in albino rats. Yet, chronic treatment of pigmented (and albino) rats for 26 weeks with compounds **1** and **2** at systemic exposures in excess of those in monkeys did not yield any evidence for retinal changes detectable with OCT, ERG, and histopathology similar to those observed in the monkey, while other types of toxicities such as to the male germ cells were congruent between albino and pigmented rats and monkeys. Hence, the retinal changes seen with chronic treatment of compounds **1** and **2** appear to be specific for the monkey, but human relevance cannot be excluded. Since accumulation in melanin-containing tissue was present in both pigmented rats and monkey, the toxicity is not directly associated with the melanin-binding potential of compounds **1** and **2**. Consolidation of the mechanism of action and judgment of whether this is a class effect would require conduct of further monkey studies with chronic treatment. Overall, the translatability of compound-induced retinal changes from cynomolgus monkeys to humans is presently unknown, but OCT was established as a highly sensitive method to detect early changes to the retina, which in our studies in cynomolgus monkeys were present after 5−6 months of treatment. Compound **1** was preferred for further clinical exploration due to its higher potency for SMN2 exon 7 inclusion and hence a potentially higher therapeutic window with respect to secondary splice target engagement, absence of safety concerns regarding phospholipidosis, phototoxicity, QT-prolongation, and an improved therapeutic window for retinal changes in the cynomolgus monkey. A full therapeutic effect is expected at exposures in patients not exceeding the no adverse effect level from animal toxicity studies.

CLINICAL EVALUATION

Compound **1**, is currently under clinical evaluation in three ongoing trials: a study in type 1 infants with SMA, a study in types 2 and 3 SMA patients age 2−25 years, and a study in non-naive SMA patients. These studies are aiming to assess safety, tolerability, and efficacy of **1** in the respective patient populations. A single ascending dose study in healthy subjects has been completed previously. The safety, pharmacokinetic, and pharmacodynamic data in human obtained so far confirm the successful optimization of the compound as described in this summary, when compared to data in human from the previous compound **2**.

CHEMISTRY

The discovery chemistry synthetic route for the preparation of compound **1** is highlighted in Scheme 1.[24] The pyridazine derivative **19** underwent a nucleophilic substitution with aqueous ammonia, giving a mixture of regioisomers which were not separated at this stage. A subsequent N-alkylation of with 1-bromo-2,2-dimethoxypropane followed by an intramolecular cyclization gave the imidazopyridazine **20** (both regioisomers were separated), which was readily converted into boronic ester **21**. In a convergent manner, a condensation between the 5-fluoropyridin-2-amine **22** and dimethyl malonate, followed by chlorination with $POCl_3$, afforded **23**. A Suzuki cross coupling between **21** and **23** led to **24**. Finally, a regioselective aromatic nucleophilic substitution with 4,7-diazaspiro[2,5]octane gave the final derivative **1**.

CONCLUSIONS

RNA splice modifiers are a new class of small molecule therapeutics. In terms of specificity and safety they represent profound challenges for medicinal chemistry. In-depth characterization of compound **2**, our first SMN2 splicing modifier which entered human clinical trials, and understanding of its safety and pharmacokinetics limitations mainly based on nonclinical data have led to the rational discovery of **1** displaying a superior profile, which is currently being verified in clinical trials. Additionally, our small molecule, unlike an ASO (which required an intrathetical administration and have a limited tissue distribution), is orally available and displayed a wide tissue

DOI: 10.1021/acs.jmedchem.8b00741
J. Med. Chem. XXXX, XXX, XXX−XXX

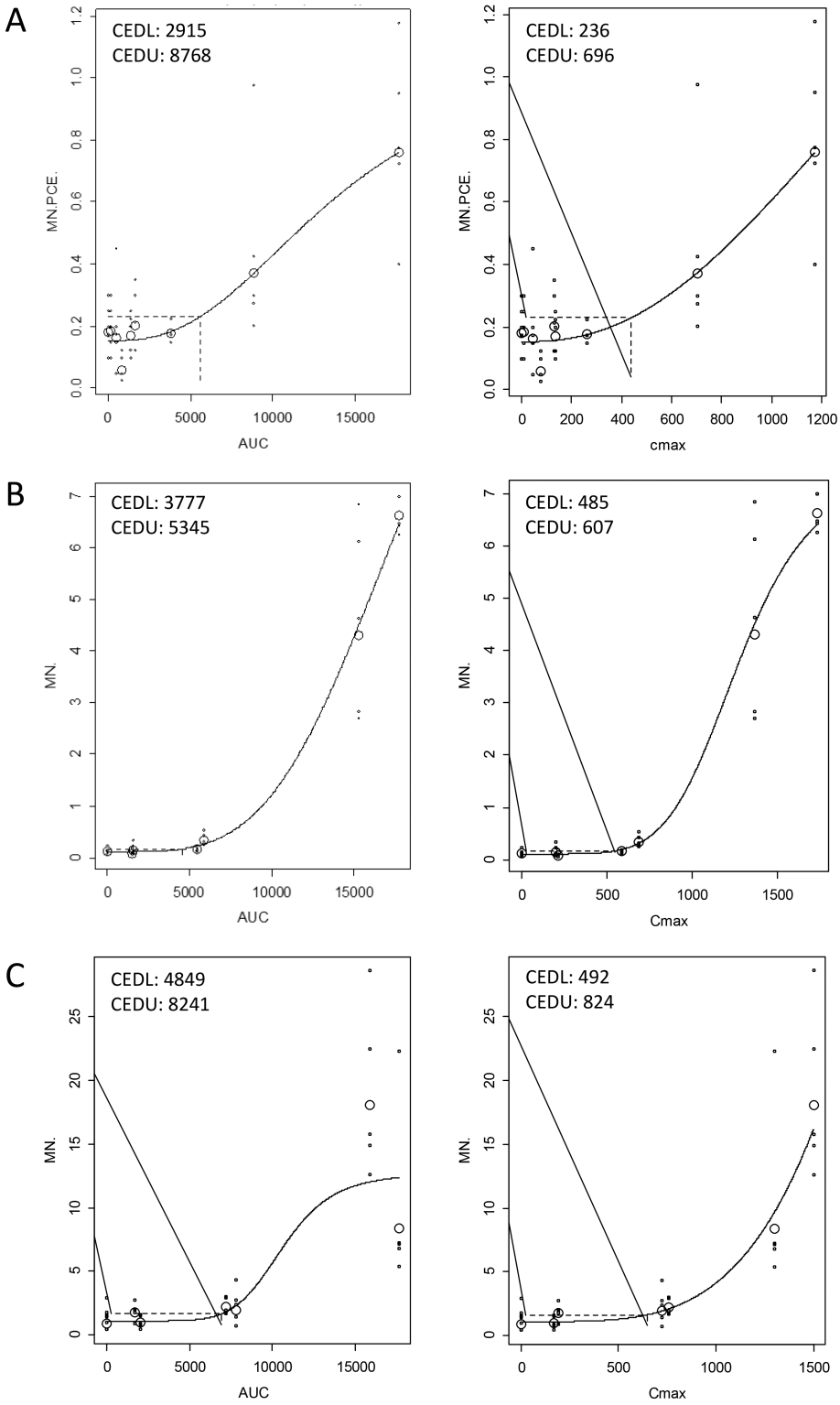

Figure 15. (A) BMD of AUC_{0-24h} (left) and C_{max} (right) vs MN in acute (48 h) study with adult rats; (B) BMD of AUC_{0-24h} (left) and C_{max} (right) vs MN in 4 week study in adult rats; (C) BMD of AUC_{0-24h} (left) and C_{max} (right) vs MN in 13 week study with juvenile rats. CES 50% (i.e., 1.5-fold increase over concurrent controls) was used with PROAST software. CEDL and CEDU are the critical size lower and upper confidence limits.

distribution. A partly novel optimization process was used, clearly beyond standard screening. Some critical standard parameters included potency both in vitro and in vivo, volume of distribution, and general safety considerations like genotoxicity, hERG channel, phototoxicity, and phospholipidosis. Beyond standard efforts included a genome-wide splice site and gene expression analysis to assess the selectivity, verification of this in induced pluripotent stem cells of man and monkey, and analysis of several organs from toxicity studies in rodents and monkeys. Eventually, the clear association between pharmacology and toxicity phenotypes in vitro and in vivo led to an elucidation of both the unique mechanism of action of our class

DOI: 10.1021/acs.jmedchem.8b00741
J. Med. Chem. XXXX, XXX, XXX−XXX

Scheme 1. Discovery Chemistry Synthetic Route of Compound 1[a]

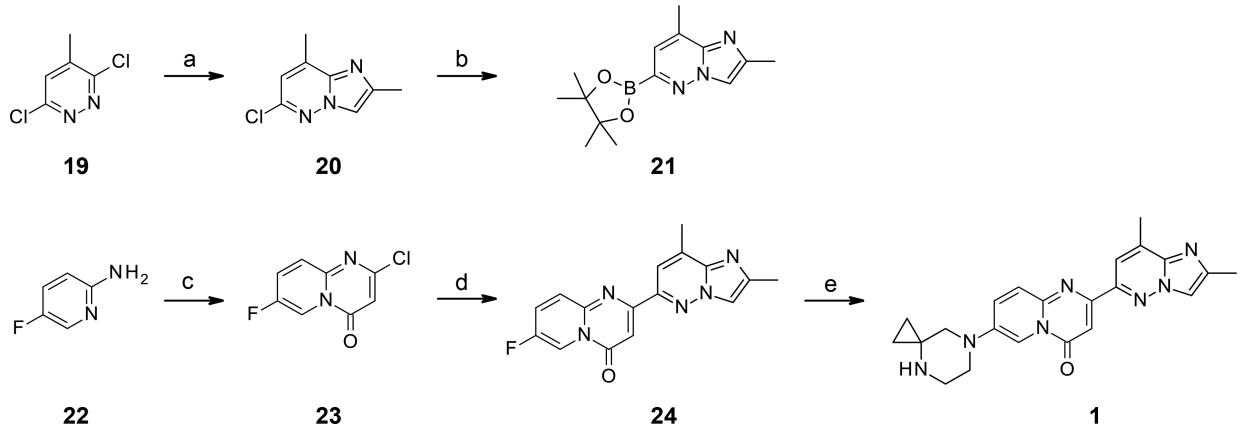

[a]Conditions: (a) (i) aqueous ammonia, 110 °C, 48 h; (ii) 1-bromo-2,2-dimethoxypropane (1.2 equiv), PPTS (0.072 equiv), 2-propanol, 105 °C, 12 h, 21% over 2 steps; (b) 4,4,4′,4′,5,5,5′,5′-octamethyl-2,2′-bi(1,3,2-dioxaborolane) (1.0 equiv), KOAc (2.0 equiv), dioxane, 110 °C; (c) (i) dimethyl malonate (5 equiv), 230 °C, 1.5 h; (ii) $POCl_3$, *i*-Pr_2NEt (1.0 equiv), 110 °C, 15 h, 50% over 2 steps; (d) **21** (1.2 equiv), $Pd(PPh_3)_4$ (0.05 equiv), aqueous K_2CO_3 (2M, 3.0 equiv), CH_3CN, 100 °C, 6.0 h, 60%; (e) 4,7-diazaspiro[2,5]octane dihydrochloride (3.0 equiv), *i*-Pr_2NEt (4.0 equiv), DMSO, 130 °C, 48 h, 18%.

of compound and the toxicity phenotypes including genotoxicity (micronucleus induction, apoptosis, and cell cycle control). Compound **1**, orally available with wide tissue distribution, suitable half-life, predictable pharmacokinetics, and very efficient in brain penetration, is currently undergoing testing in pivotal clinical trials in types 1, 2, and 3 SMA patients, with a potential for a life transformational therapy. This work enabled the selection of a drug candidate for splice modification, which can be clinically tested in patients of all ages with doses not exceeding the no observed effect levels established in extensive animal studies including juvenile animals.

The work described in this paper demonstrated that it is possible to design safe, selective, and efficacious small molecule splicing modifiers, with a potential widespread implications in the research and development of several additional RNA-targeting therapies.

EXPERIMENTAL SECTION

Nonclinical Animal Studies. All animal studies were performed under IACUC approved protocols at AAALAC-certified animal facilities.

Compound Synthesis and Characterization. Chemistry. Reactions were carried out under argon atmosphere. Unless otherwise mentioned, all reagents and chemicals were obtained from commercial suppliers and used without further purification. All reactions were followed by TLC (TLC plates F254, Merck) or LCMS (liquid chromatography−mass spectrometry) analysis. The purity of final compounds as measured by HPLC was at least above 95%. Flash column chromatography was carried out either using cartridges packed with silica gel (Isolute Columns, Telos Flash Columns) or on glass columns on silica gel 60 (32−60 mesh, 60 Å). LC high resolution spectra were recorded with a Agilent LC system consisting of Agilent 1290 high pressure system, a CTC PAL autosampler, and a Agilent 6520 QTOF. The separation was achieved on a Zorbax Eclipse Plus C18 1.7 μm, 2.1 mm × 50 mm column at 55 °C; A = 0.01% formic acid in water; B = 0.01% formic acid in acetonitrile at flow 1 mL/min with gradient 0 min 5% B, 0.3 min 5% B, 4.5 min 99% B, 5 min 99% B. The NMR spectra were measured on a Bruker 600 MHz machine in a 5 mm TCI cryoprobe at 298 K. TMS was used for referencing for experiment done in $CDCl_3$. The deuterated DMSO-d_6 solvent signal was used as reference with 2.50 ppm.

7-(4,7-Diazaspiro[2.5]octan-7-yl)-2-(2,8-dimethylimidazo-[1,2-*b*]pyridazin-6-yl)pyrido[1,2-*a*]pyrimidin-4-one (1). *According to Scheme 1: Step A. Preparation of* ***20****.* (i) In a sealed flask, 3,6-dichloro-4-methylpyridazine (27.0 g, 161 mmol) was suspended in aqueous ammonia (25%, 300 mL). The reaction mixture was heated at 110 °C for 48 h (turned into a solution after 1 h). After cooling to room temperature, the reaction was poured on CH_2Cl_2, and the organic phase was separated, dried over Na_2SO_4, concentrated under vacuum to give 22.4 g of 6-chloro-4-methylpyridazin-3-amine and 6-chloro-5-methylpyridazin-3-amine as a mixture of regioisomers which were used directly in the next step. (ii) The mixture of regioisomers was suspended in 2-propanol (300 mL). 1-Bromo-2,2-dimethoxypropane (36.0 g, 26.6 mL, 193 mmol) and PPTS (2.96 g, 11.6 mmol) were added, and the resulting solution was heated at 105 °C overnight. The volatiles were removed under vacuo, and the residue was taken up in CH_2Cl_2 and washed with $NaHCO_3$. The organic phases were dried over Na_2SO_4, concentrated under vacuo and the crude light brown solid was chromatographed (EtOAc/heptane 1/2 to 1/1) to give separately 6-chloro-2,7-dimethyl-imidazo[1,2-*b*]pyridazine (5.9 g, 20%) and 6-chloro-2,8-dimethylimidazo[1,2-*b*]pyridazine **20** (6.1 g, 21%) as a white solid. ^{1}H NMR (600 MHz, DMSO-d_6) δ ppm 8.04 (d, J = 0.6 Hz, 1H), 7.20 (d, J = 1.1 Hz, 1H), 2.54 (d, J = 1.1 Hz, 3H), 2.38 (d, J = 0.7 Hz, 3H); ^{13}C NMR (151 MHz, DMSO-d_6) δ ppm 145.0, 143.0, 138.1, 137.7, 117.0, 114.8, 15.9, 14.5. LC−HRMS: m/z = 182.0490 [(M + H)$^+$ calcd for $C_8H_9ClN_3$, 182.0485; Diff 0.5 mDa].

Step B. Preparation of ***21****.* A mixture of 6-chloro-2,8-dimethyl-imidazo[1,2-*b*]pyridazine (0.9 g, 4.96 mmol), 4,4,4′,4′,5,5,5′,5′-octamethyl-2,2′-bi(1,3,2-dioxaborolane) (1.26 g, 4.96 mmol), KOAc (0.97 g, 9.91 mmol), and Pd(dppf)Cl_2·CH_2Cl_2 (363 mg, 0.49 mmol) in dioxane (50 mL) was degassed and heated under argon at 110 °C. After 15 h, the mixture was diluted with EtOAc, filtered through Celite, and concentrated under vacuum to give 2,8-dimethyl-6-(4,4,5,5-tetramethyl-1,3,2-dioxaborolan-2-yl)imidazo[1,2-*b*]pyridazine **21** which was used directly in the next step.

Step C. Preparation of ***23****.* (i) A mixture of 2-amino-5-fluoropyridine **22** (11.20 g, 0.10 mol) and dimethyl malonate (57.0 mL, 0.50 mol) was heated at 230 °C for 1.5 h. After cooling to rt, the precipitate was collected by filtration and washed with CH_3CN to give 7-fluoro-2-hydroxy-4*H*-pyrido[1,2-*a*]pyrimidin-4-one as a light brown solid, which was used directly in the next step. (ii) A mixture of crude 7-fluoro-2-hydroxy-4*H*-pyrido[1,2-*a*]pyrimidin-4-one in $POC1_3$ (50 mL) and *i*-Pr_2NEt (13.3 mL, 77 mmol) was heated at 110 °C for 15 h. The volatiles were removed and the dark residue was treated with ice−water, washed with water (3×), and dried to give a brown solid. The crude brown solid was purified by column chromatography (SiO_2, CH_2C1_2/MeOH 95:5) to give 2-chloro-7-fluoropyrido[1,2-*a*]-pyrimidin-4-one **23** (9.84 g, 50%) as a yellow solid. ^{1}H NMR (600

DOI: 10.1021/acs.jmedchem.8b00741
J. Med. Chem. XXXX, XXX, XXX−XXX

MHz, DMSO-d_6) δ ppm: 8.99 (dd, J = 4.7, 2.9 Hz, 1H), 8.25 (ddd, J = 9.8, 7.1, 2.9 Hz, 1H), 7.85 (dd, J = 9.7, 5.3 Hz, 1H), 6.56 (s, 1H). ^{13}C NMR (151 MHz, DMSO-d_6) δ ppm 156.7 (td, J = 1.3, 0.5 Hz), 156.3 (d, J = 1.9 Hz), 154.4 (d, J = 243.6 Hz), 148.4 (d, J = 1.0 Hz), 131.4 (d, J = 25.0 Hz), 127.7 (d, J = 8.0 Hz), 114.3 (d, J = 41.6 Hz), 100.9. LC–HRMS: m/z = 199.0067 [(M + H)$^+$ calcd for $C_8H_5ClFN_2O$, 199.0074; Diff 0.7 mDa].

Step D. Preparation of ***24***. To a solution of 2-chloro-7-fluoro-4*H*-pyrido[1,2-*a*]pyrimidin-4-one **23** (750 mg, 3.78 mmol) in ACN (36 mL) were added 2,8-dimethyl-6-(4,4,5,5-tetramethyl-1,3,2-dioxaborolan-2-yl)imidazo[1,2-*b*]pyridazine **21** (1.24 g, 4.53 mmol), Pd(Ph_3P)$_4$ (218 mg, 0.189 mmol), and an aqueous solution of K_2CO_3 (3.78 mL, 7.55 mmol). The mixture was degassed and heated under argon at 100 °C for 6 h. The reaction was cooled down to rt and filtered. The precipitate was washed with Et_2O and then water, dried under vacuo to give 2-(2,8-dimethylimidazo[1,2-*b*]pyridazin-6-yl)-7-fluoropyrido[1,2-*a*]pyrimidin-4-one **24** (700 mg, 60%) as a light brown solid. ^{1}H NMR (600 MHz, DMSO-d_6) δ ppm 9.03 (dd, J = 4.7, 2.9 Hz, 1 H), 8.21 (ddd, J = 9.8, 7.1, 2.9 Hz, 1 H), 8.17 (s, 1 H), 7.98 (br s, 1 H), 7.98 (ddd, J = 9.8, 5.5, 0.6 Hz, 1 H), 7.18 (s, 1 H), 2.65 (s, 3 H), 2.44 (s, 3 H); ^{13}C NMR (151 MHz, DMSO-d_6) δ = 157.1, 156.4, 154.4 (d, J = 243.5 Hz), 149.2, 147.7, 143.7, 139.1, 135.7, 130.3 (d, J = 25.3 Hz), 128.7 (d, J = 8.0 Hz), 114.8, 114.3, 113.7 (d, J = 41.5 Hz), 98.2, 16.3, 14.6. LC–HRMS: m/z = 310.1098 [(M + H)$^+$ calcd for $C_{16}H_{13}FN_5O$, 310.1104; Diff 0.6 mDa].

Step E. Preparation of ***1***. In a sealed tube, 2-(2,8-dimethylimidazo-[1,2-*b*]pyridazin-6-yl)-7-fluoropyrido[1,2-*a*]pyrimidin-4-one **24** (50 mg, 0.162 mmol), *i*-Pr_2NEt (0.22 mL, 1.29 mmol), and 4,7-diazaspiro[2.5]octane dihydrochloride (32 mg, 0.320 mmol) were heated in DMSO (2 mL) at 130 °C for 48 h. The solvent was removed under high vacuum. The residue was taken up in CH_2Cl_2 and washed with an aqueous saturated solution of $NaHCO_3$. The organic layer was separated and dried over Na_2SO_4 and concentrated under vacuo. The crude was purified by column chromatography (SiO_2, CH_2Cl_2/MeOH = 98/2 to 95/5) to afford 7-(4,7-diazaspiro[2.5]octan-7-yl)-2-(2,8-dimethylimidazo[1,2-*b*]pyridazin-6-yl)pyrido[1,2-*a*]pyrimidin-4-one **1** (12 mg, 18%) as a pale yellow solid. ^{1}H NMR (600 MHz,$CDCl_3$) δ ppm 8.45 (d, J = 2.4 Hz, 1H), 7.92 (d, J = 1.0 Hz, 1H), 7.73 (d, J = 9.6 Hz, 1H) 7.80 (s, 1H), 7.70 (dd, J = 9.7, 2.5 Hz, 1H), 7.38 (s, 1H), 3.31–3.22 (m, 2H), 3.20–3.16 (m, 2H), 3.08 (s, 2H), 2.74 (d, J = 0.9 Hz, 3H) 2.55 (s, 3H), 1.68 (br s, 1H), 0.77–0.75 (m, 2H), 0.67–0.64 (m, 2 H); ^{13}C NMR (151 MHz,$CDCl_3$) δ ppm 158.2, 156.3, 148.5, 147.2, 144.1, 142.2, 140.0, 135.6, 131.2, 126.7, 114.9, 114.7, 110.1, 99.3, 56.7, 49.9, 44.5, 36.5, 16.9, 15.0, 13.0. LC–HRMS: m/z = 402.2051 [(M + H)$^+$ calcd for $C_{22}H_{24}N_7O$, 402.2042; Diff 0.9 mDa].

SMN HTRF Assay. The level of SMN protein in lysates of compound-treated cells was quantified as described previously.[7]

Lipophilicity (log *D*) Determination. The log *D* was measured as previously described.[9]

Ab Initio Calculation. Density functional calculations were performed using B3LYP/6-31G**. The Jaguar package (release 2017-4, Schrödinger, LLC, New York, NY) was used for all calculations.[25] The initial conformation was assigned by OPLS force-field minimization. For calculating the torsion profiles, a relaxed coordinate scan around the dihedral of interest was performed with a 5° increment.

cpKa Calculation. The calculation of the pK_a values were done using MoKa 2.0,[26] which was trained with an in-house proprietary pK_a training set.

Neuromuscular Pathology. Neuromuscular pathology was examined as described previously.[7]

■ ASSOCIATED CONTENT

Supporting Information

The Supporting Information is available free of charge on the ACS Publications website at DOI: 10.1021/acs.jmedchem.8b00741.

^{1}H NMR and ^{13}C NMR of **1** (PDF)

Molecular formula strings and some data (CSV)

■ AUTHOR INFORMATION

Corresponding Authors

*H.R.: e-mail, hasane.ratni@roche.com; phone, (+41) 61-688-2748.

*L.M.: e-mail, lutz.mueller@roche.com; phone, (+41) 61-688-2733.

ORCID

Hasane Ratni: 0000-0002-8151-8295

Author Contributions

H.R. was the discovery chemistry project leader and designed risdiplam. L.M. was the nonclinical safety leader.

Notes

The authors declare no competing financial interest.

■ ACKNOWLEDGMENTS

We thank Thierry Meyer, Serge Burner, Virginie Brom, Anke Kurt, and Heidi Schar for the synthesis of the compounds described, Josef Schneider for the NMR spectroscopy, Christian Bartelmus for the mass spectroscopy, Liudmila Polonchuk for hERG assessment, Stephan Kirchner for MNT characterization, Katja Heinig for BioAnalysis, Massimiliano Donzelli for plasma protein binding, Mohammed Ullah for P-gp assay, and Claudia Senn for in vivo PK studies in rodents and cynomolgus monkeys. Beyond these, the authors of this paper specifically extend their gratitude to the extended teams at the F. Hoffmann-La Roche R&D Innovation Center Basel, who supported these research and development activities in various functions with great enthusiasm to generate a potentially efficacious and safe medicine for SMA patients. The research described in the manuscript was funded by F. Hoffmann-La Roche AG, PTC Therapeutics, and the SMA Foundation.

■ ABBREVIATIONS USED

AUC_{0-24h}, area under the curve from 0 to 24 h; CEDL/U, critical effect dose lower/upper confidence limit; DMA, *N*,*N*-dimethylacetamide; DMAP, *N*,*N*-dimethylpyridin-4-amine; DMF, *N*,*N*-dimethylformamide; DMSO, dimethyl sulfoxide; Dppp, bis(diphenylphosphino)propane; ip, intraperitoneal; MN, micronucleus; NMR, nuclear magnetic resonance; P-gp, P-glycoprotein; PPTS, pyridinium *p*-toluenesulfonate; rt, room temperature; SMA, spinal muscular atrophy; SMN, survival of motor neuron; TFA, trifluoroacetic acid; THF, tetrahydrofuran

■ REFERENCES

(1) *Spinal Muscular Atrophy: Disease Mechanism and Theraphy*, 1st ed.; Sumner, C. J., Paushkin, S., Ko, C. P., Eds.; Academic Press: Cambridge, MA, 2016.

(2) (a) Pearn, J. Classification of Spinal Muscular Atrophies. *Lancet* **1980**, *315*, 919–922. (b) Crawford, T. O.; Pardo, C. A. The Neurobiology of Childhood Spinal Muscular Atrophy. *Neurobiol. Dis.* **1996**, *3*, 97–110. (c) Sugarman, E. A.; Nagan, N.; Zhu, H.; Akmaev, V. R.; Zhou, Z.; Rohlfs, E. M.; Flynn, K.; Hendrickson, B. C.; Scholl, T.; Sirko-Osadsa, D. A.; Allitto, B. A. Pan-Ethnic Carrier Screening and Prenatal Diagnosis for Spinal Muscular Atrophy: Clinical Laboratory Analysis of >72,400 Specimens. *Eur. J. Hum. Genet.* **2012**, *20*, 27–32.

(3) (a) Fallini, C.; Bassell, G. J.; Rossoll, W. Spinal Muscular Atrophy: The Role of SMN in Axonal mRNA Regulation. *Brain Res.* **2012**, *1462*, 81–92. (b) Schrank, B.; Gotz, R.; Gunnersen, J. M.; Ure, J. M.; Toyka, K. V.; Smith, A. G.; Sendtner, M. Inactivation of the Survival Motor Neuron Gene, a Candidate Gene for Human Spinal Muscular Atrophy, Leads to Massive Cell Death in Early Mouse Embryos. *Proc. Natl. Acad.*

DOI: 10.1021/acs.jmedchem.8b00741
J. Med. Chem. XXXX, XXX, XXX–XXX

Sci. U. S. A. **1997**, *94* (18), 9920−9925. (c) Paushkin, S.; Gubitz, A. K.; Massenet, S.; Dreyfuss, G. The SMN Complex, an Assemblyosome of Ribonucleoproteins. *Curr. Opin. Cell Biol.* **2002**, *14* (3), 305−312.

(4) Crawford, T. O.; Paushkin, S. V.; Kobayashi, D. T.; Forrest, S. J.; Joyce, C. L.; Finkel, R. S.; Kaufmann, P.; Swoboda, K. J.; Tiziano, D.; Lomastro, R.; Li, R. H.; Trachtenberg, F. L.; Plasterer, T.; Chen, K. S. Evaluation of SMN Protein, Transcript, and Copy Number in the Biomarkers for Spinal Muscular Atrophy (BforSMA) Clinical Study. *PLoS One* **2012**, *7*, e33572.

(5) (a) Kaczmarek, A.; Schneider, S.; Wirth, B.; Riessland, M. Investigational Therapies for the Treatment of Spinal Muscular Atrophy. *Expert Opin. Invest. Drugs* **2015**, *24*, 867−881. (b) Scoto, M.; Finkel, R. S.; Mercuri, E.; Muntoni, F. Therapeutic Approaches for Spinal Muscular Atrophy (SMA). *Gene Ther.* **2017**, *24* (9), 514−519. (c) Groen, E. J. N.; Talbot, K.; Gillingwater, T. H. Advances in Therapy for Spinal Muscular Atrophy: Promises and Challenges. *Nat. Rev. Neurol.* **2018**, *14* (4), 214−224.

(6) (a) Hua, Y.; Sahashi, K.; Rigo, F.; Hung, G.; Horev, G.; Bennett, C. F.; Krainer, A. R. Peripheral SMN Restoration is Essential for Long-Term Rescue of a Severe Spinal Muscular Atrophy Mouse Model. *Nature (London, U. K.)* **2011**, *478*, 123−126. (b) Passini, M. A.; Bu, J.; Richards, A. M.; Kinnecom, C.; Sardi, S. P.; Stanek, L. M.; Hua, Y.; Rigo, F.; Matson, J.; Hung, G.; Kaye, E. M.; Shihabuddin, L. S.; Krainer, A. R.; Bennett, C. F.; Cheng, S. H. Antisense Oligonucleotides Delivered to the Mouse CNS Ameliorate Symptoms of Severe Spinal Muscular Atrophy. *Sci. Transl. Med.* **2011**, *3*, 72ra18. (c) Sahashi, K.; Ling, K. K. Y.; Hua, Y.; Wilkinson, J. E.; Nomakuchi, T.; Rigo, F.; Hung, G.; Xu, D.; Jiang, Y.-P.; Lin, R. Z.; Ko, C.-P.; Bennett, C. F.; Krainer, A. R. Pathological Impact of SMN2 mis-Splicing in Adult SMA Mice. *EMBO Mol. Med.* **2013**, *5*, 1586−1601.

(7) Naryshkin, N. A.; Weetall, M.; Dakka, A.; Narasimhan, J.; Zhao, X.; Feng, Z.; Ling, K. K. Y.; Karp, G. M.; Qi, H.; Woll, M. G.; Chen, G.; Zhang, N.; Gabbeta, V.; Vazirani, P.; Bhattacharyya, A.; Furia, B.; Risher, N.; Sheedy, J.; Kong, R.; Ma, J.; Turpoff, A.; Lee, C.-S.; Zhang, X.; Moon, Y.-C.; Trifillis, P.; Welch, E. M.; Colacino, J. M.; Babiak, J.; Almstead, N. G.; Peltz, S. W.; Eng, L. A.; Chen, K. S.; Mull, J. L.; Lynes, M. S.; Rubin, L. L.; Fontoura, P.; Santarelli, L.; Haehnke, D.; McCarthy, K. D.; Schmucki, R.; Ebeling, M.; Sivaramakrishnan, M.; Ko, C.-P.; Paushkin, S. V.; Ratni, H.; Gerlach, I.; Ghosh, A.; Metzger, F. SMN2 Splicing Modifiers Improve Motor Function and Longevity in Mice with Spinal Muscular Atrophy. *Science (Washington, DC, U. S.)* **2014**, *345*, 688−693.

(8) Palacino, J.; Swalley, S. E.; Song, C.; Cheung, A. K.; Shu, L.; Zhang, X.; Van Hoosear, M.; Shin, Y.; Chin, D. N.; Keller, C. G.; Beibel, M.; Renaud, N. A.; Smith, T. M.; Salcius, M.; Shi, X.; Hild, M.; Servais, R.; Jain, M.; Deng, L.; Bullock, C.; McLellan, M.; Schuierer, S.; Murphy, L.; Blommers, M. J. J.; Blaustein, C.; Berenshteyn, F.; Lacoste, A.; Thomas, J. R.; Roma, G.; Michaud, G. A.; Tseng, B. S.; Porter, J. A.; Myer, V. E.; Tallarico, J. A.; Hamann, L. G.; Curtis, D.; Fishman, M. C.; Dietrich, W. F.; Dales, N. A.; Sivasankaran, R. SMN2 Splice Modulators Enhance U1-pre-mRNA Association and Rescue SMA mice. *Nat. Chem. Biol.* **2015**, *11*, 511−517.

(9) Ratni, H.; Karp, G. M.; Weetall, M.; Naryshkin, N. A.; Paushkin, S. V.; Chen, K. S.; McCarthy, K. D.; Qi, H.; Turpoff, A.; Woll, M. G.; Zhang, X.; Zhang, N.; Yang, T.; Dakka, A.; Vazirani, P.; Zhao, X.; Pinard, E.; Green, L.; David-Pierson, P.; Tuerck, D.; Poirier, A.; Muster, W.; Kirchner, S.; Mueller, L.; Gerlach, I.; Metzger, F. Specific Correction of Alternative Survival Motor Neuron 2 Splicing by Small Molecules: Discovery of a Potential Novel Medicine to Treat Spinal Muscular Atrophy. *J. Med. Chem.* **2016**, *59* (13), 6086−6100.

(10) Moonfish clinical study, NCT02240355. www.clinicaltrials.gov.

(11) Sivaramakrishnan, M.; McCarthy, K. D.; Huber, S.; Meier, S.; Augustin, A.; Heckel, T.; Meistermann, H.; Hug, M. N.; Birrer, P.; Schmucki, R.; Berntenis, N.; Giroud, N.; Golling, S.; Tzouros, M.; Banfai, B.; Duran-Pacheco, G.; Lamerz, J.; Luebbers, T.; Ratni, H.; Ebeling, M.; Metzger, F.; Liu, Y. H.; Krainer, A. R.; Campagne, S.; Moursy, A.; Khawaja, S.; Clery, A.; Allain, F. H. T.; Paushkin, S. Binding to SMN2 pre-mRNA-Protein Complex Elicits Specificity for Small Molecule Splicing Modifiers. *Nat. Commun.* **2017**, *8* (1), 1476.

(12) Kim, Y. H.; Choi, M. H.; Kim, J.-H.; Lim, I. K.; Park, T. J. C-Terminus-Deleted FoxM1 is Expressed in Cancer Cell Lines and Induces Chromosome Instability. *Carcinogenesis* **2013**, *34* (8), 1907−1917.

(13) (a) Ye, H.; Kelly, T. F.; Samadani, U.; Lim, L.; Rubio, S.; Overdier, D. G.; Roebuck, K. A.; Costa, R. H. Hepatocyte Nuclear Factor 3/Fork Head Homolog 11 is Expressed in Proliferating Epithelial and Mesenchymal Cells of Embryonic and Adult Tissues. *Mol. Cell. Biol.* **1997**, *17* (3), 1626−1641. (b) Chaudhary, J.; Mosher, R.; Kim, G.; Skinner, M. K. Role of Winged Helix Transcription Factor (WIN) in the Regulation of Sertoli Cell Differentiated Functions: WIN Acts as an Early Event Gene for Follicle-Stimulating Hormone. *Endocrinology* **2000**, *141* (8), 2758−2766.

(14) Pinard, E.; Green, L.; Reutlinger, M.; Weetall, M.; Naryshkin, N. A.; Baird, J.; Chen, K. S.; Paushkin, S. V.; Metzger, F.; Ratni, H. Discovery of a Novel Class of Survival Motor Neuron 2 Splicing Modifiers for the Treatment of Spinal Muscular Atrophy. *J. Med. Chem.* **2017**, *60* (10), 4444−4457.

(15) Osborne, M.; Gomez, D.; Feng, Z.; McEwen, C.; Beltran, J.; Cirillo, K.; El-Khodor, B.; Lin, M.-Y.; Li, Y.; Knowlton, W. M.; McKemy, D. D.; Bogdanik, L.; Butts-Dehm, K.; Martens, K.; Davis, C.; Doty, R.; Wardwell, K.; Ghavami, A.; Kobayashi, D.; Ko, C.-P.; Ramboz, S.; Lutz, C. Characterization of Behavioral and Neuromuscular Junction Phenotypes in a Novel Allelic Series of SMA Mouse Models. *Hum. Mol. Genet.* **2012**, *21* (20), 4431−4447.

(16) Poirier, A.; Cascais, A.-C.; Bader, U.; Portmann, R.; Brun, M.-E.; Walter, I.; Hillebrecht, A.; Ullah, M.; Funk, C. Calibration of In Vitro Multidrug Resistance Protein 1 Substrate and Inhibition Assays as a Basis to Support the Prediction of Clinically Relevant Interactions In. *Drug Metab. Dispos.* **2014**, *42* (9), 1411−1422.

(17) Le, T. T.; Pham, L. T.; Butchbach, M. E. R.; Zhang, H. L.; Monani, U. R.; Coovert, D. D.; Gavrilina, T. O.; Xing, L.; Bassell, G. J.; Burghes, A. H. M. SMNΔ7, the Major Product of the Centromeric Survival Motor Neuron (SMN2) Gene, Extends Survival in Mice with Spinal Muscular Atrophy and Associates with Full-Length SMN. *Hum. Mol. Genet.* **2005**, *14* (6), 845−857.

(18) Korver, W.; Roose, J.; Clevers, H. The Winged-Helix Transcription Factor Trident is Expressed in Cycling Cells. *Nucleic Acids Res.* **1997**, *25* (9), 1715−1719.

(19) Barann, M.; Zimmer, R.; Birzele, F. Manananggal - a Novel Viewer for Alternative Splicing Events. *BMC Bioinf.* **2017**, *18*, 120.

(20) (a) Torous, D. K.; Hall, N. E.; Murante, F. G.; Gleason, S. E.; Tometsko, C. R.; Dertinger, S. D. Comparative Scoring of Micronucleated Reticulocytes in Rat Peripheral Blood by Flow Cytometry and Microscopy. *Toxicol. Sci.* **2003**, *74* (2), 309−314. (b) Bryce, S. M.; Bernacki, D. T.; Bemis, J. C.; Spellman, R. A.; Engel, M. E.; Schuler, M.; Lorge, E.; Heikkinen, P. T.; Hemmann, U.; Thybaud, V.; Wilde, S.; Queisser, N.; Sutter, A.; Zeller, A.; Guerard, M.; Kirkland, D.; Dertinger, S. D. Interlaboratory Evaluation of a Multiplexed High Information Content In Vitro Genotoxicity Assay. *Environ. Mol. Mutagen.* **2017**, *58* (3), 146−161.

(21) MacGregor, J. T.; Frotschl, R.; White, P. A.; Crump, K. S.; Eastmond, D. A.; Fukushima, S.; Guerard, M.; Hayashi, M.; Soeteman-Hernandez, L. G.; Johnson, G. E.; Kasamatsu, T.; Levy, D. D.; Morita, T.; Muller, L.; Schoeny, R.; Schuler, M. J.; Thybaud, V. IWGT Report on Quantitative Approaches to Genotoxicity Risk Assessment II. Use of Point-of-Departure (PoD) Metrics in Defining Acceptable Exposure Limits and Assessing Human Risk. *Mutat. Res., Genet. Toxicol. Environ. Mutagen.* **2015**, *783*, 66−78.

(22) Software PROAST, version 38.9. www.rivm.nl/proast (accessed 2016).

(23) Zeller, A.; Duran-Pacheco, G.; Guerard, M. An Appraisal of Critical Effect Sizes for the Benchmark Dose Approach to Assess Dose-Response Relationships in Genetic Toxicology. *Arch. Toxicol.* **2017**, *91* (12), 3799−3807.

(24) Ratni, H.; Green, L.; Naryshkin, N. A.; Weetall, M. L. 2-(Imidazo[1,2-b]pyridazin-6-yl)pyrido[1,2a]pyrimidin-4-one Derivatives as SMN Modulators and Their Preparation and Use for the Treatment of Spinal Muscular Atrophy. WO2015173181 A1, 2015.

DOI: 10.1021/acs.jmedchem.8b00741
J. Med. Chem. XXXX, XXX, XXX−XXX

(25) Bochevarov, A. D.; Harder, E.; Hughes, T. F.; Greenwood, J. R.; Braden, D. A.; Philipp, D. M.; Rinaldo, D.; Halls, M. D.; Zhang, J.; Friesner, R. A. Jaguar: A High-Performance Quantum Chemistry Software Program with Strengths in Life and Materials Sciences. *Int. J. Quantum Chem.* **2013**, *113* (18), 2110−2142.
(26) Milletti, F.; Storchi, L.; Sforna, G.; Cruciani, G. New and Original pKa Prediction Method Using Grid Molecular Interaction Fields. *J. Chem. Inf. Model.* **2007**, *47* (6), 2172−2181.

DOI: 10.1021/acs.jmedchem.8b00741
J. Med. Chem. XXXX, XXX, XXX−XXX